DOI: 10.1002/chem.201103002

Synthesis, Computational Modeling, and Properties of Benzo-Appended BODIPYs**

Timsy Uppal,[a] Xiaoke Hu,[a] Frank R. Fronczek,[a] Stephanie Maschek,[b] Petia Bobadova-Parvanova,[b] and M. Graça H. Vicente*[a]

Abstract: A series of new functionalized mono- and dibenzo-appended BODIPY dyes were synthesized from a common tetrahydroisoindole precursor following two different synthetic routes. Route A involved the assembly of the BODIPY core prior to aromatization, while in Route B the aromatization step was performed first. In general, Route A gave higher yields of the target dibenzo-BODIPYs, due to the ease of aromatization of the BODIPYs compared with the corresponding dipyrromethenes, probably due to their higher stability under the oxidative conditions (2,3-dichloro-5,6-dicyano-1,4-benzoquinone in refluxing toluene). However, due to the slow oxidation of highly electron-deficient BODIPY **3c** bearing a *meso*-C_6F_5 group, dibenzo-BODIPY **4c** was obtained, in 35% overall from dipyrromethane, only by Route B. Computational calculations performed at the 6-31G(d,p) level are in agreement with the experimental results, showing similar relative energies for all reaction intermediates in both routes. In addition, BODIPY **3c** had the highest molecular electrostatic potential (MEPN), confirming its high electron deficiency and consequent resistance toward oxidation. X-ray analyses of eight BODIPYs and several intermediates show that benzannulation further enhances the planarity of these systems. The π-extended BODIPYs show strong red-shifted absorptions and emissions, about 50–60 nm per benzoannulated ring, at 589–658 and 596–680 nm, respectively. In particular, db-BODIPY **4c** bearing a *meso*-C_6F_5 group showed the longest λ_{max} of absorption and emission, along with the lowest fluorescence quantum yield (0.31 in CH_2Cl_2); on the other hand monobenzo-BODIPY **8** showed the highest quantum yield (0.99) of this series. Cellular investigations using human carcinoma HEp2 cells revealed high plasma membrane permeability for all dibenzo-BODIPYs, low dark- and photo-cytotoxicities and intracellular localization in the cell endoplasmic reticulum, in addition to other organelles. Our studies indicate that benzo-appended BODIPYs, in particular the highly stable *meso*-substituted BODIPYs, are promising fluorophores for bioimaging applications.

Keywords: aromatization · cellular uptake · cytotoxicity · dyes/pigments · fluorescence · planarity

Introduction

Borondipyrromethene (BODIPY) dyes, often referred to as "semi-porphyrins",[1] are among the most recent investigated fluorescence dyes for a variety of analytical and imaging applications.[2,3] Due to their favorable photophysical and optoelectronic properties that include high photostability, high extinction coefficients, and high fluorescence quantum yields, BODIPYs have attracted special interest in drug discovery,[4] biomedical imaging,[5] and optical sensing.[6,7] The success of these applications rely on the syntheses of long-wavelength absorbing and emitting BODIPYs (ca. 600–800 nm), for reduced rotational motion and fluorescence quenching,[8] as well as the incorporation of functionalities for increased solubility in aqueous media and/or for conjugation to target-specific molecules. Strategies toward these goals include the preparation of: 1) aza-substituted BODIPYs at the bridging *meso*-position, designated Aza-BODIPYs,[9] 2) core-modified BODIPYs bearing substituted aryl, ethynylphenyl or styryl groups,[10] and 3) functionalized BODIPYs with π-extended systems through the fusion of external aromatic rings to the β-pyrrolic positions.[11] The so-called π-extended BODIPYs form a class of highly constrained BODIPYs with rigid aromatic rings fused to the β,β′-pyrrole carbon atoms (Figure 1).[1a] In general, aromatic ring fusion at the β-pyrrolic positions provide constrained and highly planar BODIPY platforms with fluorescence in the near-IR region of the spectrum.[12,13] Current synthetic approaches to dibenzo-fused BODIPYs (db-BODIPYs)

[a] T. Uppal, Dr. X. Hu, Dr. F. R. Fronczek, Prof. M. G. H. Vicente
Department of Chemistry
Louisiana State University
Baton Rouge, LA, 70803 (USA)
Fax: (+1) 225-578-3458
E-mail: vicente@lsu.edu

[b] S. Maschek, Prof. P. Bobadova-Parvanova
Department of Chemistry
Rockhurst University
Kansas City, MO, 64110 (USA)

[**] BODIPY = Borondipyrromethene

Supporting information for this article is available on the WWW under http://dx.doi.org/10.1002/chem.201103002. It contains additional X-ray structures, UV/Vis and fluorescence data, cytotoxicity data, and NMR spectra, Cartesian coordinates of all optimized structures and schemes of the computed potential energy surfaces.

 © 2012 Wiley-VCH Verlag GmbH & Co. KGaA, Weinheim

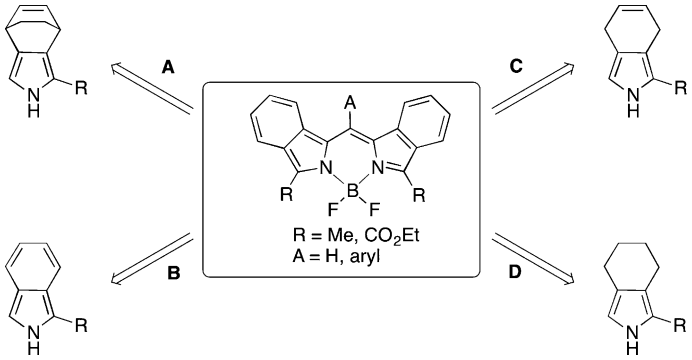

Figure 1. Synthetic strategies toward symmetric dibenzo-appended BODIPYs.

from pyrrolic precursors are shown in Figure 1. The "Ono et al. method"[2] uses a bicyclo-octadiene-fused pyrrole (Figure 1, Route A) and its major drawback is the harsh reaction conditions required for the aromatization step, upon a thermal retro Diels–Alder reaction. On the other hand the isoindole precursor required for Route B (Figure 1) is unstable due to the high reactivity of the pyrrolic α-positions. Alternatively, di- and/or tetra-hydroisoindole precursors can be used (Routes C and D), as already demonstrated for the synthesis of tetrabenzoporphyrins (TBP),[14] but these strategies have not yet been developed into a general approach toward the synthesis of benzo-BODIPY systems. While this article was in preparation, reports describing the synthesis of π-extended dipyrrins from a 4,7-dihydroisoindole precursor,[15] and an alternative synthesis of db-BODIPYs from 2-acetylphenols were published.[16] In the search of practical and straightforward approaches to benzo-appended BODIPYs, we investigated two synthetic routes from a common dipyrromethane precursor, readily available from a thermodynamically stable tetrahydroisoindole synthon (Scheme 1). Our goals were to develop a general synthetic methodology to db-BODIPYs, and to study the effect of number of fused benzene subunits and the nature of *meso*-substituent (A) on the photophysical and biological properties of BODIPYs.

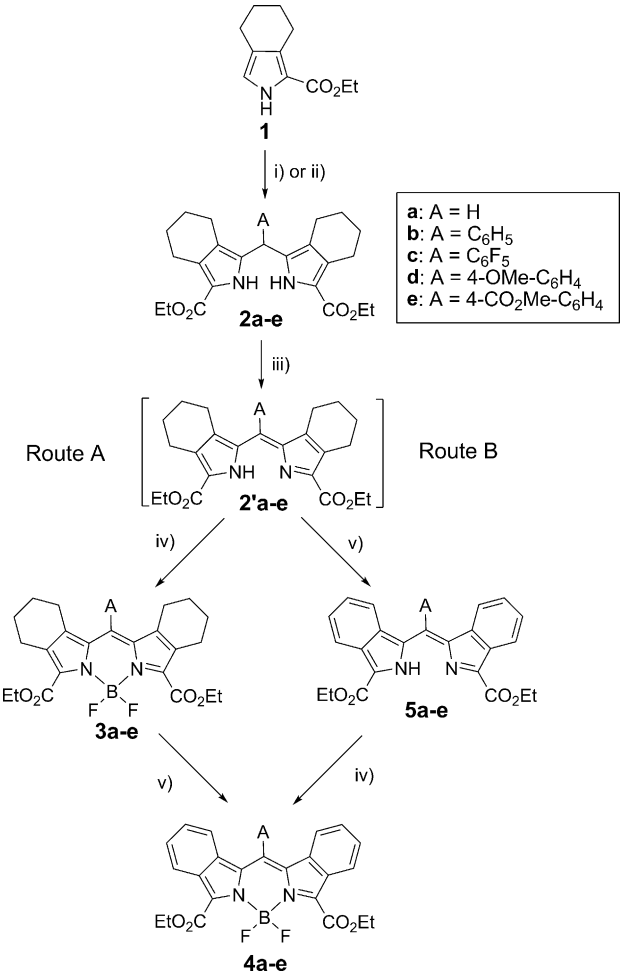

Scheme 1. Reaction conditions: i) $CH_2(OMe)_2$, TsOH, HOAc, RT, 24 h (92%); ii) Ar-CHO, TsOH, CH_2Cl_2, Bu_4Cl, RT, 12 h, (70-95%); iii) DDQ (1.2 equiv), dry CH_2Cl_2, 0°C, 20 min; iv) Et_3N, $BF_3{\cdot}OEt_2$, 0°C, 30 min to overnight, RT (55-90%); v) DDQ (9 equiv), dry toluene, reflux, 45 min to 4 h (56-92%).

Results and Discussion

Synthesis of benzo-BODIPYs: The key synthetic precursors to BODIPYs **4a–e**, dipyrromethanes **2a–e**, were prepared in high yields by acid-catalyzed condensation of aldehydes with ethyl-4,5,6,7-tetrahydroisoindole ester **1**[17] (generated using the Barton–Zard reaction) according to a modified literature procedure.[18] Two synthetic routes were investigated for the generation of db-BODIPYs **4a–e**, as shown in Scheme 1. In Route A, the BODIPY core was assembled first after mild oxidation of **2a–e** to the corresponding dipyrromethenes **2′a–e** and reaction with $BF_3{\cdot}OEt_2$ in a one-flask two-step procedure, followed by aromatization with 2,3-dichloro-5,6-dicyano-1,4-benzoquinone (DDQ), similar to the TBP synthetic methodology. The bicyclo-BODIPYs (abbreviated here as bc-BODIPYs) **3a–e** were obtained as green solids from the corresponding dipyrromethanes **2a–e** in 60–80% yields, after purification by column chromatography on silica gel and recrystallization from dichloromethane/hexanes mixtures. All bc-BODIPYs with the exception of **3c**, produced the corresponding fluorescent db-BODIPYs **4a,b,d,e** as deep blue solids in 67–92% yields, upon DDQ oxidation in refluxing toluene. The highest aromatization yield was obtained for BODIPY **4d** (92%), bearing the electron-donating 4-methoxyphenyl group, and the lowest for BODIPY **4c** (0%, even upon prolonged heating in the presence of a large excess of DDQ) bearing the strong electron-withdrawing pentafluorophenyl group. It is possible that the highly electron-deficient BODIPY **3c** has a much slower rate of oxidation, due to its lower tendency to form a benzylic cation intermediate, either by single-electron transfer, or through hydride transfer, to DDQ.[19]

These results are in agreement with previous observations on metallo-TBP synthesis, showing that metalloporphyrins

 © 2012 Wiley-VCH Verlag GmbH & Co. KGaA, Weinheim

containing electron-withdrawing *meso*-substituents have decreased aromatization reaction rates, leading to lower yields of the target products.[20] Additional oxidizing agents and reaction conditions were investigated for the aromatization step, including $KMnO_4$/K10 clay, $AgNO_3$/acetone, and $FeCl_3$/methanol, but lower yields for the target db-BODIPYs were obtained.

In Route B (Scheme 1) dipyrromethanes **2a–e** were first subjected to oxidative dehydrogenation with DDQ in refluxing toluene affording the π-extended benzodipyrrins **5a–e** as deep green crystals. The yields obtained for the oxidation reactions of **2a–e** (56-69%) or **2′a–e** (53-65%) to the corresponding benzodipyrrins **5a–e** were lower than those obtained from BODIPYs **3a,b,d,e** to **4a,b,d,e** (67–92%), with the exception of **3c** probably due to its high electron-deficiency.[19] Reaction of dipyrrins **5a–e** with $BF_3{\cdot}OEt_2$ and triethylamine in refluxing toluene[21] afforded all the target db-BODIPYs **4a–e** in 55–90% yields. These are similar to the yields obtained (60–80%) from complexation of boron to **2** or **2** by means of Route A. Although db-BODIPY **4c** could only be prepared by Route B, in general Route A gave higher overall yields for the target db-BODIPYs (41–67% from **2**) compared with Route B (31–62% from **2**) due to the easier aromatization of BODIPYs **3** (67–92%) compared with the corresponding dipyrromethenes **2′** (53–65%); this result is probably due to the higher stability of BODIPYs **3** compared with the corresponding intermediates **2** and **2** under the oxidative reaction conditions, and consequently lower tendency for formation of side products. The highest overall yield was obtained for BODIPY **4d** bearing the electron-donating 4-methoxyphenyl group, and the lowest for BODIPY **4c** bearing the strongest electron-withdrawing pentafluorophenyl group, suggesting that electron-rich bc-BODIPYs are easier to aromatize (vide infra).

In order to investigate the effect of number of fused benzene rings on the photophysical properties of BODIPYs, we also prepared monobenzo-fused BODIPY **8** (Scheme 2), following a route similar to Route A in Scheme 1. Tetrahydroisoindole ester **1**[17] and 5-formyl-pyrrole **6**[22] reacted in the presence of $POCl_3$ to produce the corresponding dipyrromethene, which reacted with $BF_3{\cdot}OEt_2$ in a one-flask two-step procedure producing BODIPY **7** in 40% overall yield.[21] Aromatization using DDQ (5 equiv) in refluxing toluene for 20 min generated the target BODIPY **8** as a green solid in 60% yield.

The structures of all compounds synthesized were confirmed by ^1H and ^{13}C NMR spectroscopy, MS, and X-ray analysis (see Supporting Information). For all the BODIPYs, single crystals suitable for X-ray structure analysis (Figures 2 and 3) were obtained by slow diffusion of hex-

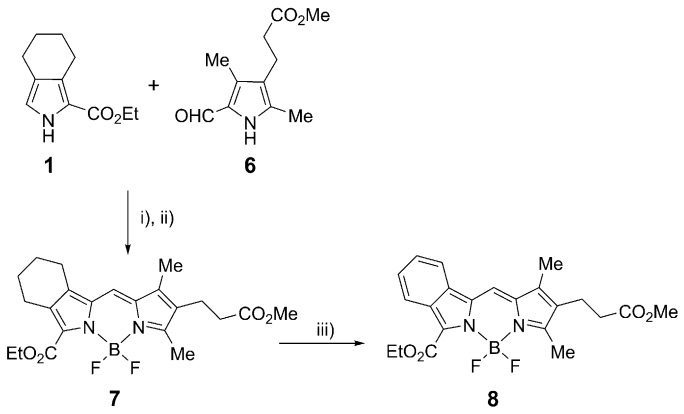

Scheme 2. Reaction conditions: i) $POCl_3$, CH_2Cl_2, 24 h, RT; ii) Et_3N, $BF_3{\cdot}OEt_2$, CH_2Cl_2, 24 h, RT (40% for two steps); iii) DDQ, toluene, reflux, 10 min (60%).

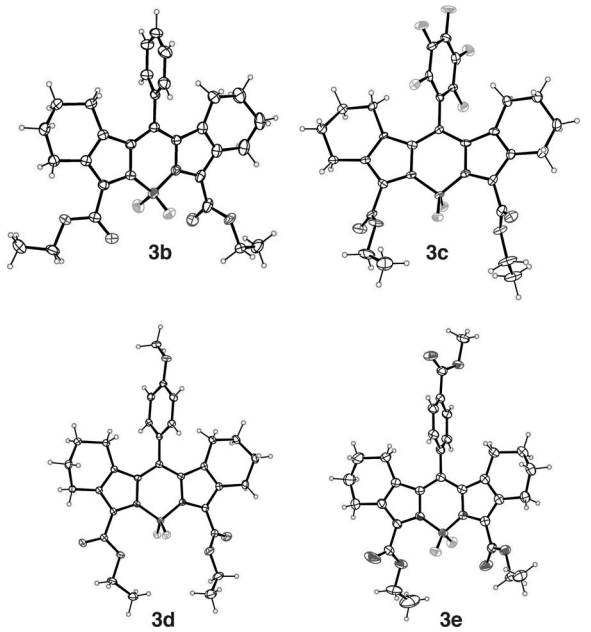

Figure 2. Molecular structures of BODIPYs **3b**, **3c**, **3d** and **3e**.

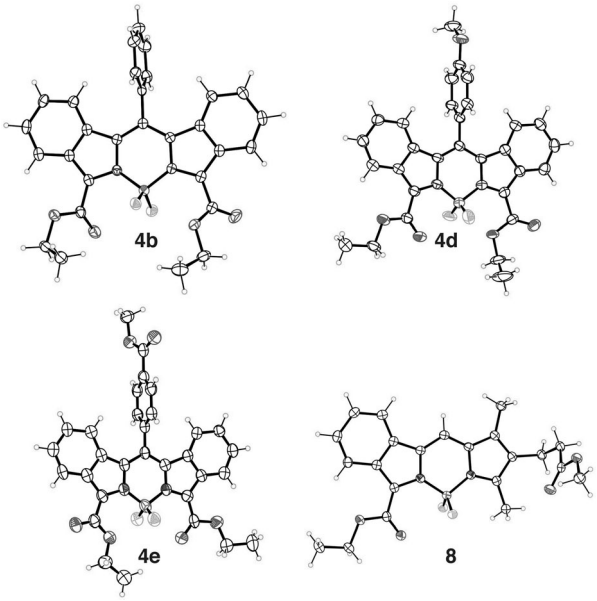

Figure 3. Molecular structures of BODIPYs **4b**, **4d**, **4e** and **8**.

 © 2012 Wiley-VCH Verlag GmbH & Co. KGaA, Weinheim

anes into a solution of compound in dichloromethane. Several molecular structures were also obtained for BODIPY precursors, and these are shown in the Supporting Information (Figures S1 and S2). Due to the central sp^3 C atom and the presence of two NH groups, the two pyrrole rings of the dipyrromethanes **2a–d** are markedly nonparallel (Figure S1). In these compounds, dihedral angles formed by the two pyrrole rings fall in the range 53.2(1)–86.01(5)°, with average value 68.5°. Both the coordination to BF_2 in the BODIPYs (Figures 2 and 3) and the intramolecular hydrogen bond formation in the dipyrromethenes (Figure S2 in the Supporting Information) cause the pyrrole rings to be more coplanar. The dihedral angles in the **3b–e** BODIPYs have an average value of 7.7°, in the benzo-BODIPYs **4b**,**d**,**e** and **8** an average value of 4.5°, and in the benzo-dipyrromethenes **5b–d** an average value of 7.0°. In the corresponding dipyrromethenes with saturated 6-rings (see Figure S2), dihedral angles have an average value of 8.6°. Thus, from the average values, pyrrole rings in benzo-dipyrromethenes tend to be slightly more coplanar than in their saturated derivatives, the same is true of the corresponding BODIPYs, and the BODIPYs tend to exhibit slightly higher coplanarity than their free-pyrrole analogs. These trends generally also hold, with a few exceptions, when comparing individual pairs of compounds for which we have determined both crystal structures. These include three pairs of benzo- versus saturated BODIPYs and five pairs of BODIPYs versus their uncoordinated analogs.

Computational studies: The computational comparison between the two reaction routes, Routes A and B, were aimed at examining the effect of different *meso*-substituents on reaction energetics. Four different aryl substituents were used: C_6H_5, C_6F_5, 4-OMe-C_6H_4, and 4-CO_2Me-C_6H_4, corresponding to structures **2b–e, 2′b–e, 3b–e**, **4b–e**, and **5b–e**, respectively. Calculated relative energies are listed in Table 1 and in Scheme S1 of the Supporting Information. As can be seen, there is no significant difference when different substituents are used. The energy differences are between 1 and 4 kcal mol^{-1}, whereas the accuracy of thermochemical calculations is generally considered to be around 1 kcal mol^{-1}. Therefore, thermodynamically there is no observable difference when different aryl substituents are used. This result indicates that the significant differences in the yields obtained experimentally for the target BODIPYs **4b–e** are probably a result of different potential energy barriers.

To examine the solvent effect, structures **2b, 2′b, 3b**, **4b**, and **5b** were re-optimized in dichloromethane and toluene, respectively, since reactions **2**→**2** and **2**→**3** were carried out in dichloromethane, while reactions **3**→**4**, **2**→**5**, and **5**→**4**, were carried out in toluene. The results are shown in Table 2. The presence of the solvent stabilizes all structures.

Table 1. Relative energies [kcal mol^{-1}] of BODIPY reaction species following the two synthetic routes when different substituents are used.

		Substituent			
	BODIPY	C_6H_5	C_6F_5	4-OMe-C_6H_4	4-CO_2Me-C_6H_4
Route A					
reactant	**2**	0	0	0	0
intermediate	**2′**	−14	−13	−15	−14
intermediate	**3**	−8	−6	−9	−7
product	**4**	−127	−124	−124	−126
Route B					
reactant	**2**	0	0	0	0
intermediate	**5**	−138	−136	−135	−137
product	**4**	−127	−124	−124	−126

Table 2. Relative energies [kcal mol^{-1}] of BODIPY reaction species following the two synthetic routes with and without the accounting of the solvent effect. The solvent is dichloromethane for reaction **2**→**2′**, triethanolamine for **2′b**→**3b** and **5b**→**4b**, and toluene for **3b**→**4b** and **2b**→**5b**.

	BODIPY	In gas-phase	In solvent
Route A			
reactant	**2b**	0	0
intermediate	**2′b**	−14	−16
intermediate	**3b**	−8	−8
product	**4b**	−127	−131
Route B			
reactant	**2b**	0	0
intermediate	**5b**	−138	−145
product	**4b**	−145	−136

However, in Route A the effect on the relative energies is rather small—between 2–4 kcal mol^{-1} and close to the calculation error. In Route B the effect is more pronounced, especially for step 2. The presence of toluene affects the energetics of step 2 with only 2 kcal mol^{-1}, but step 1 by 7 kcal mol^{-1}. Thus, in overall Route B is 9 kcal mol^{-1} more exothermic in toluene solvent than in gas phase mainly due to the increased exothermicity of step 1. The performed in-solvent calculations suggest that in general, modeling of the reaction in gas phase will give a realistic description. However, care must be taken when Route B, step 1 is studied. For this step solvent effects are more pronounced and result in higher exothermicity than in gas phase.

In order to obtain further insight on the different reactivity observed between **2b–e** (or **2′b–e**) and **3b–e**, we investigated the properties of the cyclohexenyl hydrogen atoms in these molecules by calculating the average molecular electrostatic potentials at their nuclei (MEPN). This data are summarized in Table 3. The calculated MEPN showed significant differences when different *meso*-aryl substituents were used. The third place after the decimal point is reliable and can be used for tendency examination. The comparison

Table 3. Average molecular electrostatic potential at nuclei (MEPN) at the cyclohexenyl hydrogen atoms of **2′b–e**, **3b–e**, and **2b–e**.

Dipyrromethene	$MEPN_H$	BODIPY	$MEPN_H$	Dipyrromethane	$MEPN_H$
2′b	−1.136	**3b**	−1.128	**2b**	−1.137
2′c	−1.128	**3c**	−1.120	**2c**	−1.132
2′d	−1.138	**3d**	−1.130	**2d**	−1.138
2′e	−1.134	**3e**	−1.126	**2e**	−1.135

© 2012 Wiley-VCH Verlag GmbH & Co. KGaA, Weinheim

of MEPN data clearly indicates that dipyrromethenes **2′**, in general, have more negative MEPNs compared with the corresponding BODIPYs **3**, making them less electron-deficient and more likely to undergo oxidation. Therefore, the higher yields obtained from oxidation of **3b,d,e** compared with **2b,d,e** and **2′b,d,e** are probably due to the higher stability of BODIPYs and their lower tendency to undergo side reactions. On the other hand, the calculated MEPN for BODIPY **3c** has the highest value of all MEPNs, suggesting that this compound is too electron-deficient to undergo oxidation, according to the experimental observations.

Spectroscopic properties: The photophysical properties of BODIPYs **3a–e**, **4a–e**, **7** and **8** were investigated in dichloromethane, toluene, and in a protic solvent (methanol) and the results are summarized in Tables 4 and S1 (Supporting Information). Figures 4, S3 and S4 (Supporting Information) show the normalized absorption and fluorescence spectra obtained for the benzo-appended BODIPYs, in dichloromethane, methanol, and toluene, respectively. All BODIPYs showed absorptions with high molar absorption coefficients ($\log\varepsilon = 3.5$–4.4) and relatively narrow fluorescence emission bands in the three solvents, characteristic of this type of compound.[23] The strong BODIPY absorption bands are due to the S_0–S_1 (π–π^*) transition, and the shoulders at low wavelength are due to the 0–1 vibrational transition, as previously reported.[23,24]

In dichloromethane and toluene, the absorption bands for the BODIPY core, monobenzo- and dibenzo-appended BODIPYs were centered at about 540, 590 nm and 640 nm, respectively, and the fluorescence emission maxima at about 560, 595 nm and 665 nm, respectively. Changing the solvent polarity from dichloromethane to methanol, caused 4–7 nm blue-shifts of the absorption and emission bands, in agreement with previous reports.[23] As expected, benzannulation caused a large bathochromic shift in the absorption and emission bands, of about 50–60 nm per ring, in both solvents. For example, the aromatization of **7** to produce monobenzo-BODIPY **8** lead to nearly a 60 nm red-shift in the absorption and emission bands, whereas dibenzannulation from **3a** to **4a** lead to an approximate 90 nm red-shift (Table 4). Even larger bathochromic shifts were observed for the BODIPYs bearing a *meso*-aryl group, for example, about 104 nm from **3b,d,e** to **4b,d,e**, respectively. Furthermore, BODIPY **3c** and **4c** bearing a strongly electron-withdrawing pentafluorophenyl group showed absorption and emission bands red-shifted by about 20 nm compared with the other 8-aryl substituted BODIPYs, indicating a better stabilization of the LUMO and decreased HOMO–LUMO energy gap.[24] However, the change in the *para*-phenyl substituent (H, OMe or CO_2Me) only caused 1–4 nm

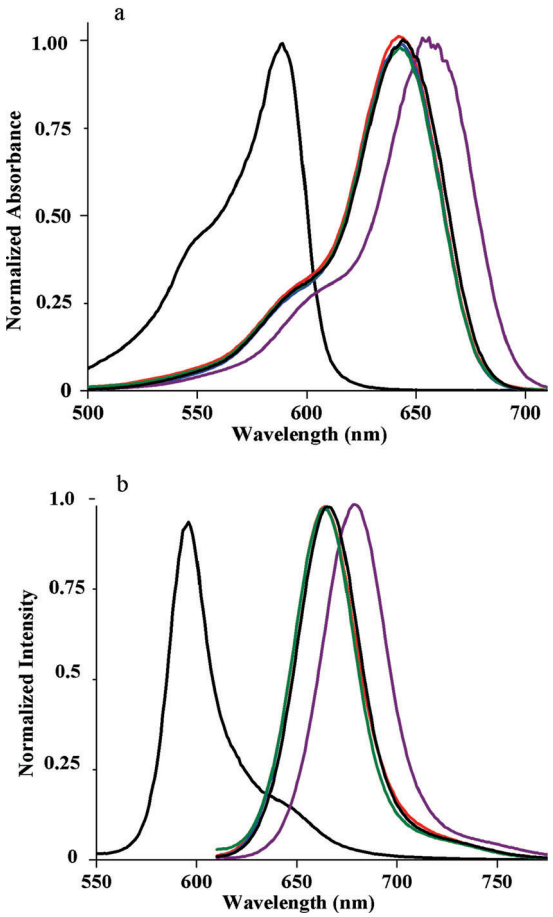

Figure 4. Normalized UV/Vis (a) and fluorescence (b) spectra of BODIPYs **8** (black), **4a** (red), **4b** (blue), **4c** (purple), **4d** (green) and **4e** (brown) in dichloromethane at 25 °C.

Table 4. Spectral properties of BODIPYs **3a–e**, **4a–e**, **7** and **8** in dichloromethane and methanol (in parenthesis), at room temperature.

	Absorbance λ_{max} [nm]	ε [$M^{-1}cm^{-1}$]	Emission λ_{max} [nm]	Φ_f[a]	Stokes shift [cm^{-1}]
3a	553 (545)	10700 (11300)	567 (562)	0.35 (0.23)	446 (555)
3b	540 (535)	20300 (21700)	561 (555)	0.34 (0.29)	693 (673)
3c	563 (557)	10700 (12500)	586 (579)	0.18 (0.06)	697 (682)
3d	539 (535)	17600 (22800)	559 (556)	0.34 (0.20)	664 (706)
3e	542 (538)	17300 (20500)	562 (560)	0.30 (0.22)	656 (730)
4a	642 (635)	19800 (3300)	664 (651)	0.38 (0.11)	516 (387)
4b	643 (635)	24400 (17200)	665 (654)	0.38 (0.45)	515 (457)
4c	658 (652)	19200 (nd)	680 (nd)	0.31 (nd)	492 (nd)
4d	643 (635)	15300 (18600)	664 (655)	0.43 (0.38)	492 (481)
4e	644 (636)	26300 (8800)	666 (654)	0.43 (0.36)	513 (433)
7	530 (523)	20700 (28500)	541 (536)	0.53 (0.32)	384 (464)
8	589 (582)	14900 (16700)	596 (591)	0.99 (0.77)	199 (262)

[a] Fluorescence quantum yields for BODIPYs **7** ($\lambda_{exc} = 481$ nm) and **3** ($\lambda_{exc} = 500$ nm) were calculated using rhodamine 6G (0.80 in methanol) as standard, while those for BODIPY **8** ($\lambda_{exc} = 530$ nm) and **4** ($\lambda_{exc} = 600$ nm) were calculated using cresyl violet perchlorate (0.54 in ethanol) and methylene blue (0.03 in mehanol) as the reference,[29] respectively.

© 2012 Wiley-VCH Verlag GmbH & Co. KGaA, Weinheim

shifts in the absorption/emission maxima, in agreement with previous observations.[25]

The fluorescence quantum yields determined in dichloromethane were higher for the db-BODIPYs **4** (0.31–0.43) compared with the corresponding bc-BODIPYs **3** (0.18–0.35). The highest quantum yields, 0.53 and 0.99, were determined for BODIPYs **7** and **8**, respectively, probably due to the presence of a methyl rather than a carbonyl group at the pyrrolic α-position,[2,26] and the lowest for BODIPY **3c**. The lower fluorescence quantum yields observed for BODIPYs **3c** and **4c** could be due to additional aryl group rotation[25a,27] and/or to the heavy atom effect,[25] although recently high fluorescence quantum yields were reported for a α,α′-dimethyl-BODIPY bearing a *meso*-C_6F_5 group, and its derivatives.[28] The fluorescence quantum yields determined in non-polar toluene varied between 0.60 (for **4c**) and 0.96 for BODIPY **8** (Table S1, Supporting Information). In methanol, the fluorescence quantum yields were generally observed to decrease probably due to an increase in the rate of non-radiative deactivation in a more polar solvent.[25] The ester groups at the pyrrolic α-positions of BODIPYs **3**, **4**, **7**, and **8** confer water solubility for the biological investigations (vide infra) but generally decrease fluorescence quantum yields, compared with for example, a methyl group, because of the relative high flexibility of the ethoxy carbonyl substituent.

Cellular studies: The dark and phototoxicity of BODIPYs **4a–e**, and **8** toward human carcinoma HEp2 cells was evaluated using the Cell Titer Blue assay, and the results are summarized in Table 5 and Figures S6 and S7 (in the Supporting Information). Although BODIPYs **4a–e** contain two α-ethoxy carbonyl substituents, they were poorly soluble in water and required dimethyl sulfoxide (DMSO) and Cremophor EL as delivery vehicles (never exceeding 0.9% DMSO/0.1% Cremophor).[30] All BODIPYs were found to have very low cytotoxicities, with half maximal inhibitory concentrations (IC_{50}) (dark) > 200 μM and IC_{50} (ca. 1.5 J cm^{-2} light dose) > 100 μM. BODIPY **4b** was found to have the highest dark toxicity of this series, probably due to its lower solubility compared with the other BODIPYs, particularly at the higher concentrations investigated during the dark toxicity experiments. The low cytotoxicity of the BODIPY dyes is in agreement with previous investigations, which report dark IC_{50} values > 100 μM for a series of 15 BODIPYs in three cell lines, with exception of a few iodinated derivatives.[31]

Table 5. Cytotoxicity (Cell Titer Blue assay, light dose ca. 1.5 J cm^{-2}) and subcellular localization (HEp2 cells) for benzo-appended BODIPYs.

BODIPY	Dark toxicity IC_{50} [μM]	Phototoxicity IC_{50} [μM]	Major sites of localization
4a	> 400	> 100	ER, Lyso, Golgi, Mito
4b	236	> 100	ER, Mito
4c	> 400	> 100	ER, Lyso, Mito
4d	> 400	> 100	ER, Lyso, Golgi, Mito
4e	373.5	> 100	ER, Lyso, Golgi
8	400	> 100	ER, Mito

The time-dependent uptake of BODIPYs was also evaluated at a concentration of 10 μM over a period of 24 h (Figure 5). BODIPY **4c** bearing a pentafluorophenyl group, was clearly taken-up by HEp2 cells to a higher extent than all other BODIPYs, at all time points investigated. This observation is probably due to the polar hydrophobic nature of the fluorinated BODIPY **4c**, which enhances plasma membrane permeability and increases cellular uptake.[32] The *meso*-free monobenzo- and dibenzo-BODIPYs **8** and **4a** accumulated the least within cells, probably due to their lower stability compared with the *meso*-substituted db-BODIPYs. It has been reported that the presence of a *meso*-aryl group increases the photostability of BODIPYs.[6a] Significant fluorescence quenching of BODIPYs **8** and **4a** was observed in DMSO with time, as shown in Figure S4 of the Supporting Information. However no fluorescence quenching was observed under the same conditions for the *meso*-substituted BODIPYs **4b–e**. After 24 h the amount of BODIPY **4c** found within cells was about 4 times higher than that of **4a** and about 40 times higher than that of **8**.

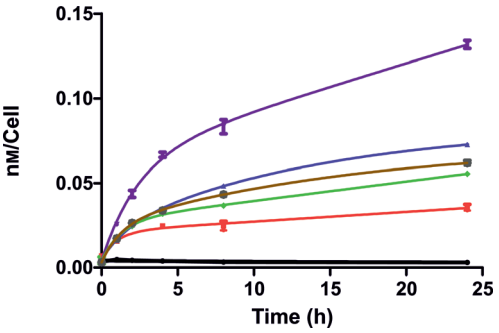

Figure 5. Time-dependent uptake of BODIPYs **8** (black), **4a** (red), **4b** (blue), **4c** (purple), **4d** (green) and **4e** (brown) at 10 μM by HEp2 cells.

The subcellular localization of BODIPYs was investigated using fluorescence microscopy and the results obtained are shown in Figures 6 and 7 and summarized in Table 5. The organelle specific fluorescent probes ERTracker (ER), LysoSensor Green (lysosomes), Mitotracker Green (mitochondria) and BODIPY Ceramide (Golgi) were used in the overlay experiments. All BODIPYs were found to localize in the ER. This result is in agreement with previous observations that BODIPYs bearing alkyl and aryl groups tend to localize in the cell ER.[33] In addition, **4a–d** and **8** were also found in mitochondria, **4a** and **4c–e** in the lysosomes and **4a** and **4d,e** in the Golgi. Our results are in agreement with literature reports showing that BODIPYs readily accumulate within cells,[31,33,34] and can be found in multiple organelles, including the ER, Golgi, mitochondria and lysosomes. Commercially available BODIPYs are known for the specific labeling of Golgi and/or the ER, for example BODIPY FL Ceramide.[3b] The low cytotoxicity, high photostability

© 2012 Wiley-VCH Verlag GmbH & Co. KGaA, Weinheim

and plasma membrane permeability of benzo-BODIPYs suggest that these compounds could be used for drug delivery into cells, or as cation sensors within living cells, in particular the *meso*-aryl-substituted benzo-BODIPYs.

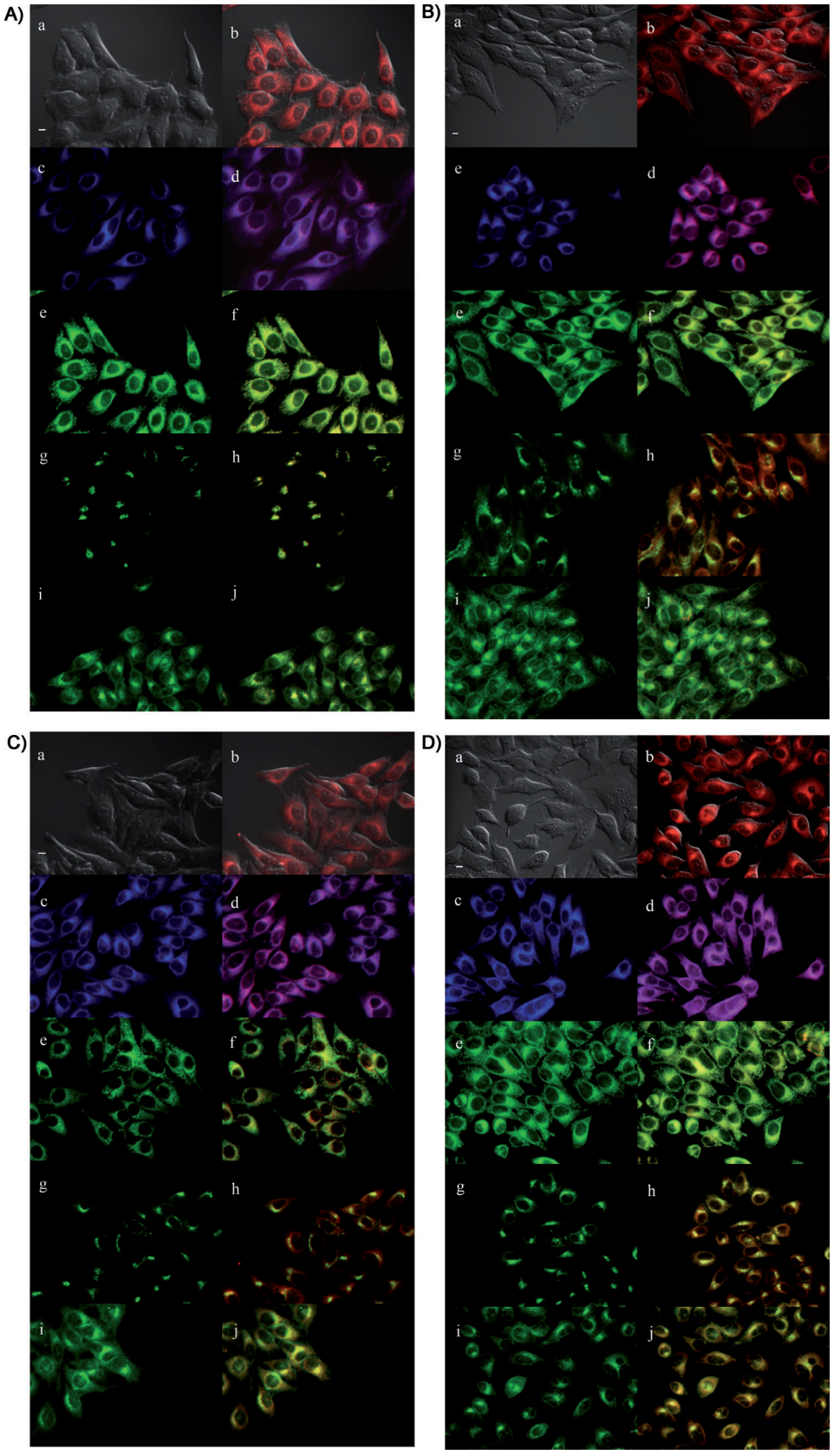

Conclusion

Two alternative synthetic routes were investigated for the preparation of π-extended BODIPYs bearing β,β′-fused benzene rings, with fluorecence emissons in the 596–680 nm region, from a common intermediate. Route A involved boron complexation to the dipyrromethene ($BF_3{\cdot}OEt_2/NEt_3$), followed by aromatization with DDQ in refluxing toluene. In Route B the aromatization step to the corresponding dibenzodipyrromethenes was performed first, followed by complexation with boron. In general, Route A gave higher yields of the dibenzo-BODIPYs (41–67 % from dipyrromethane **2**) because of the higher yields obtained from aromatization of the BODIPYs compared with the corresponding dipyrromethenes; this might be due to the higher stability of the BODIPYs under the oxidative reaction conditions. There was however one exception (BODIPY **4c**), due to the slow oxidation rate of the highly electron-deficient **3c**, bearing a *meso*-pentafluorophenyl group; in this case, dibenzo-BODIPY **4c** was rather obtained by Route B, in 35 % overall yield from dipyrromethane **2**. Computational model-

Figure 6. Subcellular localization of A) BODIPY **4a** B) BODIPY **4b**, C) BODIPY **4c**, and D) BODIPY **4d** in HEp2 cells at 10 μM for 6 h. a) Phase contrast, b) overlay of the BODIPY fluorescence and phase contrast, c) ER tracker blue/white fluorescence, e) MitoTracker green fluorescence, g) BODIPY Ceramide, i) LysoSensor green fluorescence, and d), f), h), and j) overlays of organelle tracers with the BODIPY fluorescence. Scale bar: 10 μm.

© 2012 Wiley-VCH Verlag GmbH & Co. KGaA, Weinheim

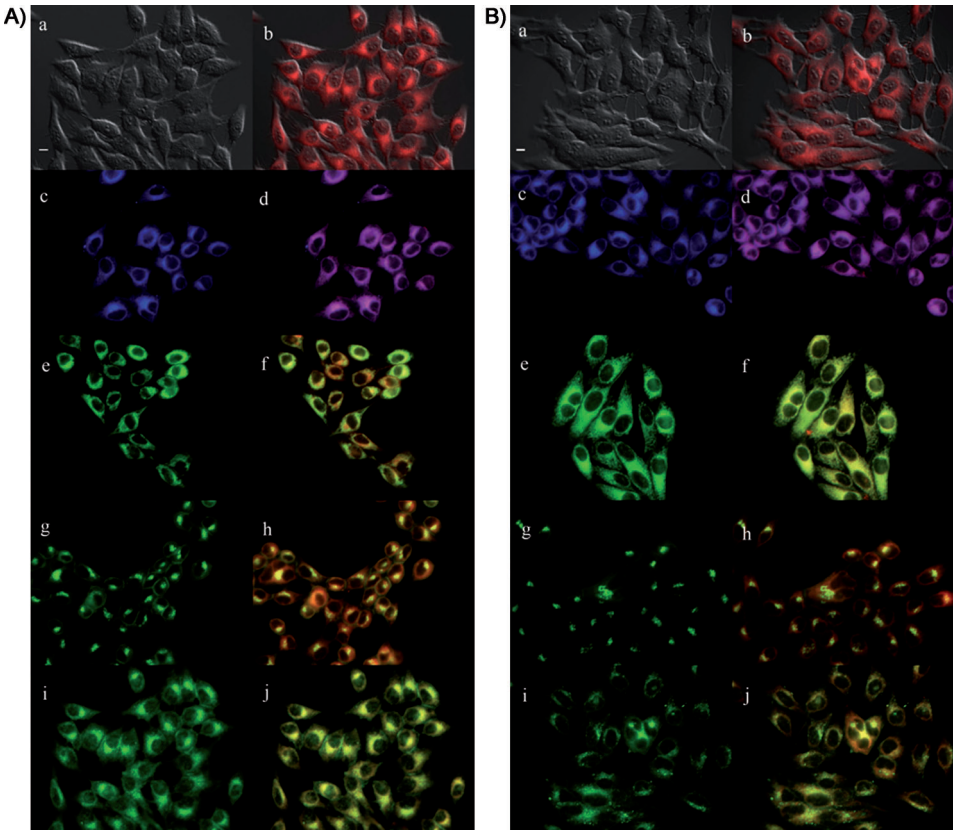

Figure 7. Subcellular localization of A) BODIPY **4e** and B) BODIPY **8** in HEp2 cells at 10 μM for 6 h. a) Phase contrast, b) overlay of the BODIPY fluorescence and phase contrast, c) ER tracker Blue/White fluorescence, e) MitoTracker Green fluorescence, g) BODIPY Ceramide, i) LysoSensor Green fluorescence, and d), f), h), and j) overlays of organelle tracers with the BODIPY fluorescence. Scale bar: 10 μm.

ing of both synthetic approaches demonstrated that changing the *meso*-substituents did not influence significantly the energetics of the reaction regardless of the route; therefore thermodynamically there was no significant difference when different substituents are used. Furthermore, for Route B the solvent effects were more pronounced and resulted in higher exothermicity for the overall reaction. The calculated MEPN for the butano hydrogen atoms of BODIPY **3c** confirmed the high electron-deficiency of this compound (highest MEPN), which might explain its stability under the oxidation reaction conditions. On the other hand, X-ray analyses of several BODIPYs and intermediates showed that benzannulation further enhances the coplanarity of BODIPY systems.

The π-extended BODIPYs all showed strong red-shifted absorptions and fluorescence emissions, about 50–60 nm per benzoannulated ring. The dibenzo-BODIPY **4c** bearing a *meso*-pentafluorophenyl group showed the longest λ_{max} absorption and emission, together with the lowest fluorescence quantum yield (0.31 in CH_2Cl_2); on the other hand monobenzo-BODIPY **8** showed the highest quantum yield (0.99), probably due to the presence of a methyl rather than the more flexible ethoxycarbonyl group at the pyrrolic α-position. The π-extended BODIPYs **4a–e**, and **8** showed very low dark- and phototoxicities toward human HEp2 cells with estimated IC_{50} values above 100 μM. BODIPY **4c** bearing a pentafluorophenyl group accumulated within the HEp2 cells the most of all BODIPYs investigated, while **8** accumulated the least followed by **4a**, probably due to their lower stability compared with the *meso*-aryl dibenzo-BODIPYs. All BODIPYs localized in the cell ER, and in addition were also found in other organelles, such as mitochondria, lysosomes and Golgi. Our results suggest that benzo-appended BODIPYs, in particular the *meso*-substituted BODIPYs, are promising fluorophores for bioimaging applications.

Experimental Section

Syntheses. All air and moisture sensitive reactions were performed under argon atmosphere in oven-dried glassware. Common reagents were obtained from commercial source and used without further purification, unless otherwise stated. Dry solvents were collected from PS-400 Solvent Purification System from Innovative Technology, Inc. Melting points were determined in open capillary and are uncorrected. Column chromatography was performed on silica gel (Sorbent Technologies, 60 Å, 40–63 μm) slurry packed into glass columns. Analytical thin-layer-chromatography (TLC) was carried out using polyester backed TLC plates 254 (precoated, 200 μm, Sorbent Technologies). ^{1}H NMR and ^{13}C NMR spectra were recorded on Bruker DPX-400 (operating at 400 MHz for ^{1}H NMR and 100 MHz for ^{13}C NMR) in $CDCl_3$ (7.26 ppm, ^{1}H and 77.0 ppm,^{13}C) with tetramethylsilane as internal standard. All spectra were recorded at 25 °C and coupling constants (*J* values) are given in Hz. Chemical shifts are given in parts per million (ppm). High resolution mass spectra were obtained at the LSU Department of Chemistry Mass Spectrometry Facility using an ESI or MALDI-TOF method, and a peak matching protocol to determine the mass error range of the molecular ion. Ethyl 4,5,6,7-tetrahydroisoindole ester (**1**)[17] 5-formyl-pyrrole **6**[22] and bis(3-ethoxycarbonyl-4,5,6,7-tetrahydro-2H-isoindolyl)methane (**2a**)[17a] were synthesized as previously described.

General procedure for the synthesis of 8-aryl-bis(3-ethoxycarbonyl-4,5,6,7-tetrahydro-2*H*-isoindolyl)methanes (2b–e): Pyrrole **1** (0.1007 g, 0.5 mmol) was treated with *p*-toluenesulfonic acid (0.0047 g, 0.025 mmol), *n*-tetrabutylammonium chloride (0.0036 g, 0.01 mmol) and THE corresponding aldehyde (0.3 mmol) in CH_2Cl_2 (50 mL). The mixture was stirred overnight at room temperature under inert atmosphere, washed with aqueous saturated $NaHCO_3$ (2×30 mL), brine (1×30 mL) and dried over anhydrous Na_2SO_4. The solvent was evaporated under vacuum and the resulting residue was chromatographed on a silica gel column (elution: hexanes/ethyl acetate 5:1 for **2b, 2d, 2e** and hexanes/ethyl acetate 7:3 for **2c**). The product was recrystallized from CH_2Cl_2/hexanes.

*Data for **2b***: Yield 117 mg (95%); m.p. 110–112 °C; ^{1}H NMR ($CDCl_3$): δ = 8.74 (br s, 2H), 7.32–7.08 (m, 5H), 5.42 (s, 1H), 4.22–4.15 (m, 4H),

© 2012 Wiley-VCH Verlag GmbH & Co. KGaA, Weinheim

2.78 (m, 4H), 2.21 (m, 4H), 1.68 (m, 8H), 1.28 ppm (t, $J=7.12$ Hz, 6H); ^{13}C NMR ($CDCl_3$): $\delta=161.8$, 139.1, 130.8, 129.2, 128.9, 128.2, 127.3, 119.7, 116.7, 59.7, 40.6, 23.3, 23.1, 21.2, 14.5 ppm; ESI-HRMS: *m/z* calcd for $C_{29}H_{34}N_2O_4$ [$M+H^+$]: 475.2575; found: 474.25.

Data for ***2c***: Yield 123 mg (87%); m.p. 106–108°C; ^{1}H NMR ($CDCl_3$): $\delta=8.71$ (brs, 2H), 5.79 (s, 1H), 4.27 (q, $J=7.12$ Hz, 4H), 2.27 (m, 4H), 2.26 (m, 2H), 2.12 (m, 2H), 1.70 (m, 8H), 1.33 ppm (t, $J=7.12$ Hz, 6H); ^{13}C NMR ($CDCl_3$): $\delta=161.4$, 146.0, 143.6, 141.9, 139.2, 139.1, 136.5, 128.9, 126.3, 120.2, 117.6, 113.4, 113.3, 113.1, 60.0, 29.8, 23.1,23.0, 22.8, 21.0, 20.1, 14.4 ppm; ESI-HRMS: *m/z* calcd for $C_{29}H_{29}F_5N_2O_4$ [$M+Na^+$]: 587.1946; found: 564.20.

Data for ***2d***: Yield 112 mg (89%); m.p. 113–116°C; ^{1}H NMR ($CDCl_3$): $\delta=9.39$ (brs, 2H), 7.91 (m, 2H), 7.15 (m, 2H), 5.50 (s, 1H), 4.18–4.06 (m, 4H), 3.91 (s, 3H), 2.74 (m, 4H), 2.26 (m, 4H), 1.69 (m, 8H), 1.24 ppm (t, $J=7.12$ Hz, 6H); ^{13}C NMR ($CDCl_3$): $\delta=166.6$, 161.9, 144.9, 130.2, 129.9, 129.2, 128.9, 128.1, 120.0, 117.2, 59.8, 52.1, 40.1, 23.3, 23.1, 23.1, 21.4, 14.4 ppm; ESI-HRMS: *m/z* calcd for $C_{30}H_{36}N_2O_5$ [$M+H^+$]: 504.2576 ; found: 504.26.

Data for ***2e***: Yield 93 mg (70%); m.p. 104–106°C; ^{1}H NMR ($CDCl_3$): $\delta=$ 8.92 (brs, 2H), 7.94 (m, 2H), 7.16 (m, 2H), 5.47 (s, 1H), 4.17 (m, 4H), 3.91 (s, 3H), 2.76 (m, 4H), 2.21 (m, 4H), 1.68 (m, 8H), 1.27 ppm (t, $J=$ 7.12 Hz, 6H); ^{13}C NMR ($CDCl_3$): δ, 166.3, 161.1, 146.2, 143.4, 142.0, 138.6, 132.3, 131.1, 129.8, 129.5, 127.6, 61.2, 52.5, 24.5, 23.2, 22.5, 21.7, 14.0 ppm; ESI-HRMS: *m/z* calcd for $C_{31}H_{36}N_2O_6$ [$M+H^+$]: 533.2649; found: 532.26.

General procedure for the synthesis of 8-aryl-bis(3-ethoxycarbonyl-4,5,6,7-tetrahydro-2*H*-isoindolyl)methenes (2′b–e): A solution of DDQ (0.36 mmol, 1.2 equiv) in dry dichloromethane (10 mL) was added to a solution of **2′b–e** (0.3 mmol, 1.0 equiv) in dry dichloromethane (20 mL) at 0°C. The solution was stirred under argon for 15–20 min until TLC analysis indicated reaction completion. The reaction mixture was washed with aqueous saturated $NaHCO_3$ (2×30 mL), brine (1×30 mL) and dried over anhydrous Na_2SO_4. The solvent was evaporated under vacuum and the residue was chromatographed on a silica gel column using CH_2Cl_2/petroleum ether 5:1 for elution. The product was recrystallized from CH_2Cl_2/hexanes.

Data for ***2′b***: Yield 106 mg (75%); m.p. 164–166°C; ^{1}H NMR ($CDCl_3$): $\delta=7.45$ (m, 3H), 7.27 (m, 2H), 4.37 (q, $J=7.12$ Hz, 4H), 2.69 (m, 4H), 1.57 (m, 4H), 1.51 (m, 4H), 1.42 (t, $J=7.12$ Hz, 6H), 1.36 ppm (m, 4H); ^{13}C NMR ($CDCl_3$): $\delta=162.3$, 143.8, 141.7, 139.7, 139.0, 137.0, 133.0, 129.1, 128.8, 128.7, 60.6, 24.2, 23.2, 23.1, 22.3, 14.4 ppm; ESI-HRMS: *m/z* calcd for $C_{29}H_{32}N_2O_4$ [$M+H^+$]: 473.2447; found: 472.2362.

Data for ***2′c***: Yield 118 mg (70%); m.p. 158–160°C; ^{1}H NMR ($CDCl_3$): $\delta=4.37$ (q, $J=7.12$ Hz, 4H), 2.67 (m, 4H), 1.67 (m, 4H), 1.60 (m, 4H), 1.52 (m, 8H), 1.41 ppm (t, $J=7.12$ Hz, 6H); ^{13}C NMR ($CDCl_3$): $\delta=161.8$, 145.8, 143.2, 138.6, 137.8, 134.0, 132.4, 127.4, 60.9, 29.4, 23.3, 23.2, 23.0, 22.8, 22.4, 22.2, 22.0, 14.1 ppm; ESI-HRMS: *m/z* calcd for $C_{29}H_{27}F_5N_2O_4$ [$M+H^+$]: 563.1978; found: 562.1891.

Data for ***2′d***: Yield 123 mg (82%); m.p. 172–174°C; ^{1}H NMR ($CDCl_3$): $\delta=7.28$ (m, 2H), 7.11 (m, 2H), 4.49 (q, $J=7.12$ Hz, 4H), 4.07 (s, 3H), 3.05 (m, 4H), 1.96 (m, 4H), 1.53 (m, 8H), 1.22 ppm (t, $J=7.12$ Hz, 6H); ^{13}C NMR ($CDCl_3$): $\delta=161.6$, 160.3, 147.2, 142.7, 139.6, 133.0, 132.1, 129.2, 126.2, 114.2, 60.6, 55.3, 24.5, 23.2, 23.1, 22.4, 14.4 ppm; ESI-HRMS: *m/z* calcd for $C_{30}H_{34}N_2O_5$ [$M+H^+$]: 503.2560; found: 502.2467.

Data for ***2′e***: Yield 108 mg (68%); m.p. 155–157°C; ^{1}H NMR ($CDCl_3$): $\delta=8.18$ (m, 2H), 8.01 (m, 2H), 4.49 (m, 4H), 3.95 (s, 3H), 2.67 (m, 4H), 1.65 (m, 4H), 1.53 (m, 4H), 1.42 (t, $J=7.12$ Hz, 6H), 1.31 ppm (m, 4H); ^{13}C NMR ($CDCl_3$): $\delta=166.3$, 162.1, 146.2, 143.6, 142.2, 138.6, 133.0, 130.1, 129.8, 129.5, 128.0, 61.2, 52.5, 24.5, 23.2, 23.1, 22.4, 14.0 ppm; ESI-HRMS: *m/z* calcd for $C_{31}H_{34}N_2O_6$ [$M+H^+$]: 531.2480; found: 530.2417.

General procedure to BODIPYs 3: A solution of DDQ (0.6 mmol, 1.2 equiv) in dry THF (10 mL) was added to a solution of **2a** (0.5 mmol, 1.0 equiv) in dry THF (10 mL) for **2a** or CH_2Cl_2 for **2b–e**, at 0°C. The solution was stirred under argon for 20 min. Et_3N (3 mmol, 6 equiv) and $BF_3{\cdot}OEt_2$ (5 mmol, 10 equiv) were added dropwise and the solution was stirred for 20 min at 0°C and then overnight at room temperature. Once TLC indicated reaction completion, the solvent was removed under reduced pressure and the residue was dissolved in ethyl acetate and extracted with 0.1 M HCl (2×30 mL) to remove excess DDQ, brine (1× 30 mL) and dried over anhydrous Na_2SO_4. The solvent was evaporated under vacuum and the resulting residue was purified by column chromatography (elution: hexanes/ethyl acetate 3:2). The product was recrystallized from CH_2Cl_2/hexanes.

Data for ***3a***: Yield 149 mg (67%); m.p. 169–171°C; ^{1}H NMR ($CDCl_3$): $\delta=5.30$ (s, 1H), 4.42 (q, $J=7.11$ Hz, 4H), 2.65 (m, 8H), 1.76 (m, 8H), 1.42 ppm (t, $J=7.11$ Hz, 6H); ^{13}C NMR ($CDCl_3$): $\delta=161.7$, 144.1, 142.6, 134.4, 132.8, 129.6, 128.7, 128.6, 126.1, 121.2, 61.6, 60.7, 29.7, 23.1, 22.9, 22.8, 22.7, 22.4, 22.0, 21.5, 14.3, 14.1, 14.0 ppm; ESI-HRMS: *m/z* calcd for $C_{23}H_{27}BF_2N_2O_4$ [$M+Na^+$]: 467.1917; found: 444.20.

Data for ***3b***: Yield 208 mg (80%); m.p. 209–211°C; ^{1}H NMR ($CDCl_3$): $\delta=7.52$ (m, 3H), 7.23 (m, 2H), 4.44 (q, $J=7.12$ Hz, 4H), 2.57 (m, 4H), 1.57 (m, 8H), 1.42 (t, $J=7.12$ Hz, 6H), 1.39 ppm (m, 4H); ^{13}C NMR ($CDCl_3$): $\delta=161.6$, 147.6, 143.8, 143.6, 134.6, 132.9, 132.5, 129.6, 129.5, 127.2, 61.7, 24.4, 22.6, 22.3, 22.0, 14.0 ppm; MALDI-TOF: *m/z* calcd for $C_{29}H_{31}BF_2N_2O_4$ [$M+Na^+$]: 543.237; found: 520.23.

Data for ***3c***: Yield 229 mg (75%); m.p. 202–204°C; ^{1}H NMR ($CDCl_3$): $\delta=4.45$ (q, $J=7.12$ Hz, 4H), 2.60 (m, 4H), 1.81 (m, 4H), 1.65 (m, 4H), 1.59 (m, 4H), 1.45 ppm (t, $J=7.12$ Hz, 6H); ^{13}C NMR ($CDCl_3$): $\delta=161.0$, 145.6, 142.3, 137.8, 133.9, 133.5, 132.6, 128.3, 62.0, 29.6, 23.3, 23.2, 23.0, 22.8, 22.4, 22.1, 22.0, 14.0 ppm; MALDI-TOF: *m/z* calcd for $C_{29}H_{26}BF_7N_2O_4$ [M^+]: 610.1876; found: 610.19.

Data for ***3d***: Yield 200 mg (73%); m.p. 181–183°C; ^{1}H NMR ($CDCl_3$): $\delta=7.12$ (m, 2H), 7.03 (m, 2H), 4.43 (q, $J=7.1$ Hz, 4H), 3.89 (s, 3H), 2.76 (m, 4H), 2.57 (m, 4H), 1.64 (m, 4H), 1.58 (m, 4H), 1.41 (t, $J=7.1$ Hz, 6H), 1.40 ppm (m, 4H); ^{13}C NMR ($CDCl_3$): $\delta=161.5$, 160.6, 147.9, 143.7, 143.4, 133.3, 132.4, 128.6, 126.5, 114.8, 61.6, 55.3, 24.7, 22.6, 22.3, 22.0, 14.0 ppm; ESI-HRMS: *m/z* calcd for $C_{30}H_{33}BF_2N_2O_5$ [$M+Na^+$]: 573.2361; found: 550.25.

Data for ***3e***: Yield 174 mg (60%); m.p. 173–175°C; ^{1}H NMR ($CDCl_3$): $\delta=8.21$ (m, 2H), 7.36 (m, 2H), 4.43 (q, $J=7.12$ Hz, 4H), 3.99 (s, 3H), 2.57 (m, 4H), 1.56 (m, 8H), 1.44 (t, $J=7.12$ Hz, 6H), 1.39 ppm (m, 4H); ^{13}C NMR ($CDCl_3$): $\delta=166.6$, 161.4, 146.0, 144.1, 143.5, 139.2, 132.8, 132.4, 131.4, 130.7, 127.6, 61.8, 52.5, 24.6, 22.5, 22.3, 21.9, 14.0 ppm; ESI-HRMS: *m/z* calcd for $C_{31}H_{33}BF_2N_2O_6$ [$M+H^+$]: 577.2299; found: 578.24.

General procedure for the synthesis of BODIPYs 4 by Route A: BODIPYs **3a–e** (112 mg, 0.2665 mmol) were dissolved in toluene (30 mL) and heated to 110°C. A solution of DDQ (9 equiv) in toluene (20 mL) was added and the final mixture was refluxed under argon. The reaction was monitored by UV/Vis spectroscopy. Upon reaction completion, the mixture was cooled to room temperature and the solvent was removed under reduced pressure. The residue was dissolved in CH_2Cl_2 (30 mL) and extracted with 10% aqueous $NaHCO_3$ (3×30 mL), brine (1×30 mL) and dried over anhydrous Na_2SO_4. The solvent was removed under reduced pressure and the residue was purified by column chromatography (elution: CH_2Cl_2 to 0.1% MeOH in CH_2Cl_2). The product was recrystallized from CH_2Cl_2/hexanes.

Data for ***4a***: Yield 81 mg (69%); m.p. >250°C; ^{1}H NMR ($CDCl_3$): $\delta=$ 8.45 (m, 2H), 8.15 (m, 2H), 7.55 (m, 2H), 7.41 (m, 2H), 4.60 (q, $J=$ 7.11 Hz, 4H), 1.55 ppm (t, $J=7.3$ Hz, 6H); ^{13}C NMR ($CDCl_3$): $\delta=160.2$, 140.2, 133.8, 130.9, 127.2, 124.5, 122.9, 62.4, 14.1 ppm; MALDI-TOF: *m/z* calcd for $C_{23}H_{27}BF_2N_2O_4$ [$M+H^+$]: 444.20; found: 444.20.

Data for ***4b***: Yield 91 mg (67%); m.p. >250°C; ^{1}H NMR ($CDCl_3$): $\delta=$ 8.11 (m, 2H), 7.72 (m, 3H), 7.52 (m, 2H), 7.26 (m, 2H), 7.08 (m, 2H), 6.16 (m, 2H), 4.62 (q, $J=7.12$ Hz, 4H), 1.55 ppm (t, $J=7.12$ Hz, 6H); ^{13}C NMR ($CDCl_3$): $\delta=160.6$, 141.2, 140.2, 134.7, 134.2, 131.2, 130.1, 129.8, 129.7, 129.1, 128.5, 126.5, 124.1, 121.7, 62.2, 14.1 ppm; ESI-HRMS: *m/z* calcd for $C_{29}H_{23}BF_2N_2O_4$ [$M+Na^+$] 535.1633; found: 512.17.

Data for ***4d***: Yield 132 mg (92%); m.p. >250°C; ^{1}H NMR ($CDCl_3$): $\delta=$ 8.11 (m, 2H), 7.26 (m, 8H), 6.30 (m, 2H), 4.61 (q, $J=7.12$ Hz, 4H), 4.02 (s, 3H), 1.55 ppm (t, $J=7.12$ Hz, 6H); ^{13}C NMR ($CDCl_3$): $\delta=160.8$, 160.6, 141.4, 139.9, 134.7, 131.1, 129.8, 129.6, 129.5, 126.4, 126.2, 124.0, 121.8, 115.1, 62.2, 55.5, 14.1 ppm; MALDI-TOF: *m/z* calcd for $C_{30}H_{25}BF_2N_2O_5$ [M^+]: 542.260; found: 542.18.

 © 2012 Wiley-VCH Verlag GmbH & Co. KGaA, Weinheim

Data for ***4e***: **Yield** 103 mg (68%); m.p. >250°C; ^{1}H NMR ($CDCl_3$): δ= 8.39 (m, 2H), 8.12 (m, 2H), 7.65 (m, 2H), 7.27 (m, 2H), 7.09 (m, 2H), 6.12 (m, 2H), 4.62 (q, J=7.12 Hz, 4H), 4.07 (s, 3H), 1.55 ppm (t, J= 7.12 Hz, 6H); ^{13}C NMR ($CDCl_3$): δ=166.3, 160.5, 140.6, 139.7, 138.8, 134.4, 131.8, 131.2, 131.0, 130.0, 128.9, 128.5, 126.7, 124.3, 121.4, 62.3, 52.6, 14.1 ppm; MALDI-TOF: m/z calcd for $C_{31}H_{25}$ $BF_2N_2O_6$ [M+H$^+$]: 570.213; found: 570.18;.

General procedure to dibenzo-fused dipyrrins (5a–e): Dipyrromethanes (**2a–e**) (112 mg, 0.2665 mmol) were dissolved in dry toluene (30 mL) and heated to 110°C. A solution of DDQ (9 equiv) in dry toluene (20 mL) was added and the mixture was refluxed under argon. The reaction was monitored by UV/Vis spectroscopy and upon completion the solvent was removed under reduced pressure. The purple residue was dissolved in ethyl acetate and extracted with 0.1 M HCl to remove traces of DDQ (3× 50 mL), brine (1×50 mL) and dried over anhydrous Na_2SO_4. The solvent was removed under reduced pressure and the residue was purified by column chromatography (elution: CH_2Cl_2 for **5a, 5b** and hexanes/ethyl acetate, 2:1 for **5c,d,e**). The product was recrystallized from CH_2Cl_2/methanol.

Data for ***5a***: Yield 57 mg (56%); m.p. 168–169°C; UV/Vis (CH_2Cl_2): λ_{max} (ε)=568 nm (13710 M^{-1}cm^{-1}); ^{1}H NMR ($CDCl_3$): δ=8.48 (m, 2H), 8.23 (m, 2H), 7.40 (m, 4H), 4.55 (q, J=7.07 Hz, 4H), 1.55 ppm (t, J=7.3 Hz, 6H); ^{13}C NMR ($CDCl_3$): δ=161.6, 137.1, 134.5, 133.3, 133.0, 131.3, 130.8, 128.7, 127.7, 127.0, 126.5, 126.4, 123.1, 123.0, 122.8, 118.9, 61.5, 61.2, 61.1, 29.6, 14.3, 14.5 ppm; ESI-HRMS: m/z calcd for $C_{23}H_{20}N_2O_4$ [M+H$^+$]: 388.14; found: 388.14.

Data for ***5b***: Yield 81 mg (66%); m.p. 146–147°C; UV/Vis (CH_2Cl_2): λ_{max} (ε)=569 nm (24136 M^{-1}cm^{-1}); ^{1}H NMR ($CDCl_3$): δ=8.19 (m, 2H), 7.66 (m, 5H), 7.24 (m, 2H), 6.97 (m, 2H), 6.12 (m, 2H), 5.30 (s, 1H), 4.58 (q, J=7.12 Hz, 4H), 1.56 ppm (t, J=7.12 Hz, 6H); ^{13}C NMR ($CDCl_3$): δ= 161.8, 137.7, 136.4, 135.5, 135.0, 131.6, 129.5, 129.4, 129.1, 126.9, 126.0, 122.8, 122.0, 61.2, 14.4 ppm; ESI-HRMS: m/z calcd for $C_{29}H_{24}N_2O_4$ [M+H$^+$]: 465.1788; found: 464.17.

Data for ***5c***: Yield 91 mg (62%); m.p. 224–225°C; UV/Vis (CH_2Cl_2): λ_{max} (ε)=583 nm (34069 M^{-1}cm^{-1}); ^{1}H NMR ($CDCl_3$): δ=8.25 (m, 2H), 7.33 (m, 2H), 7.18 (m, 2H), 6.34 (m, 2H), 4.56 (q, J=7.12 Hz, 4H), 1.56 ppm (t, J=7.12 Hz, 6H); ^{13}C NMR ($CDCl_3$): δ=161.4, 139.3, 134.6, 134.3, 131.8, 128.2, 126.8, 123.7, 119.8, 61.5, 14.4 ppm; ESI-HRMS: m/z calcd for $C_{29}H_{19}F_5N_2O_4$ [M+Na$^+$]: 555.1328; found: 554.13.

Data for ***5d***: Yield 90 mg (69%); m.p. 197–199°C; UV/Vis (CH_2Cl_2): λ_{max} (ε)=569 nm (31070 M^{-1}cm^{-1}); ^{1}H NMR ($CDCl_3$): δ=8.20 (m, 2H), 7.43 (m, 2H), 7.24 (m, 2H), 7.18 (m, 2H), 7.02 (m, 2H), 6.28 (m, 2H), 4.57 (q, J=7.12 Hz, 4H), 4.01 (s, 3H), 1.56 ppm (t, J=7.12 Hz, 6H); ^{13}C NMR ($CDCl_3$): δ=161.8, 135.7, 131.7, 130.6, 126.9, 126.0, 122.7, 122.1, 114.8, 61.2, 55.5,14.4 ppm; MALDI-TOF: m/z calcd for $C_{30}H_{26}N_2O_5$ [M+H$^+$] 495.258; found: 494.18.

Data for ***5e***: Yield 81 mg (58%); m.p. 208–209°C; UV/Vis (CH_2Cl_2): λ_{max} (ε)=572 (30918 M^{-1}cm^{-1}), ^{1}H NMR ($CDCl_3$): δ=8.35 (m, 2H), 8.18 (m, 2H), 7.65 (m, 2H), 7.23 (m, 2H), 6.96 (m, 2H), 6.06 (m, 2H), 4.57 (q, J= 7.12 Hz, 4H), 4.06 (s, 3H), 1.56 ppm (t, J=7.12 Hz, 6H); ^{13}C NMR ($CDCl_3$): δ=166.6, 161.7, 141.1, 138.1, 137.8, 135.3, 134.4, 131.7, 131.2, 130.7, 129.5, 128.8, 127.1, 126.2, 123.0, 121.7, 61.3, 52.5, 14.4 ppm; ESI-HRMS: m/z calcd for $C_{31}H_{26}N_2O_6$ [M+H$^+$] 522.1831; found: 522.18;.

General procedure for synthesis of BODIPYs 4 by Route B: A solution of db-dipyrrins **5a–e** (0.1 mmol) in toluene (20 mL) was stirred at 0°C for 15 min under argon. Et_3N (0.089 mL, 0.64 mmol) and $BF_3{\cdot}OEt_2$ (0.13 mL, 1.024 mmol) were added and the mixture was stirred at room temperature for 30 min. The reaction mixture was then refluxed until UV/Vis spectroscopy indicated reaction completion. The solution was washed with 10% aqueous $NaHCO_3$ (3×20 mL), brine (1×20 mL) and dried over anhydrous Na_2SO_4. The solvent was evaporated under reduced pressure and the product was obtained after recrystallization from CH_2Cl_2/hexanes mixtures. Yields obtained: **4a**, 24 mg (55%): **4b**, 40 mg (80%); **4c**, 34 mg (56%); **4d**, 49 mg (90%); **4e**, 43 mg (75%).

Data for **4c**: M.p. >250°C; ^{1}H NMR ($CDCl_3$): δ=8.16 (m, 2H), 7.38–7.25 (m, 4H), 6.39 (m, 2H), 4.62 (q, J=7.12 Hz, 4H), 1.54 ppm (t, J= 7.12 Hz, 6H); ^{13}C NMR ($CDCl_3$): δ=160.1, 142.0, 133.8, 131.3, 131.2, 128.5, 127.3, 125.1, 122.5, 119.5, 62.6, 14.1 ppm; MALDI-TOF: m/z calcd for $C_{29}H_{18}$ $BF_7N_2O_4$ [M^+]: 602.179; found: 602.12.

BODIPY 7: Pyrrole **1** (150 mg, 0.7762 mmol) and **6** (162 mg, 0.7762 mmol) were dissolved in dry dichloromethane (20 mL) at 0°C and $POCl_3$ (0.14 mL, 0.9314 mmol) was added dropwise over 5 min. The reaction mixture was stirred at 0°C for 10 min and then stirred overnight at room temperature. After TLC indicated reaction completion, Et_3N (0.5 mL, 3.9 mmol) was added dropwise at 0°C, followed by $BF_3{\cdot}OEt_2$ (0.8 mL, 6.2 mmol) at 0°C. After the addition was complete, the mixture was stirred for 16 h at room temperature. The solvent was removed under reduced pressure and the residue was dissolved in dichloromethane (20 mL) and washed with 10% aqueous $NaHCO_3$ (2×20 mL), brine (2×20 mL) and dried over anhydrous Na_2SO_4. The solvent was evaporated to dryness under reduced pressure and the resulting residue was purified by column chromatography (elution with hexanes/ethyl acetate 3:2). The fraction containing the product was collected, dried under vacuum and recrystallized from CH_2Cl_2/hexanes to yield pure BODIPY **7** (134 mg, 40%) as a lustrous green solid. M.p. 135–137°C; ^{1}H NMR ($CDCl_3$, 400 MHz): δ=7.04 (s, 1H), 4.37 (q, J=7.12 Hz, 4H), 3.67 (s, 1H), 2.72 (m, 4H), 2.65 (overlapped m, 2H), 2.61 (s, 3H), 2.46 (m, 2H), 2.21 (s, 3H), 1.75 (m, 1H), 1.38 ppm (t, J=7.12 Hz, 3H); ^{13}C NMR ($CDCl_3$, 100 MHz): δ=172.6, 165.5, 161.1, 141.7, 136.7, 136.5, 132.2, 131.9, 131.7, 120.8, 60.6, 51.8, 33.4, 23.3, 23.1, 22.4, 21.5, 19.4, 14.2, 13.7, 9.6 ppm; MALDI-TOF: m/z calcd for $C_{22}H_{27}BF_2N_2O_6$ [M+Na$^+$]: 455.251; found: 432.27.

BODIPY 8: BODIPY **7** (100 mg, 0.2313 mmol) was dissolved in toluene (15 mL) and heated to 110°C. A solution of DDQ (262 mg, 1.1566 mmol, 5 equiv) in toluene (15 mL) was added and the mixture was refluxed under argon. The reaction was monitored using UV/Vis. Once the reaction was complete, it was allowed to cool down to room temperature and the solvent was removed under reduced pressure. The residue was dissolved in dichloromethane (20 mL) and extracted with aqueous saturated $NaHCO_3$ (20 mL), brine (20 mL) and dried over anhydrous Na_2SO_4. The solution was evaporated to dryness and the residue was purified by column chromatography (elution: hexanes/ethyl acetate 3:2). The fractions containing the title BODIPY were collected, dried under vacuum and recrystallized from CH_2Cl_2/hexanes, yielding pure BODIPY **8** (59.4 mg, 60%) as a lustrous green solid. M.p. 162–164°C; ^{1}H NMR ($CDCl_3$, 400 MHz): δ=8.22 (m, 1H), 7.79 (m, 1H), 7.46 (s, 1H), 7.41 (m, 1H), 7.34 (m, 1H), 4.55 (q, J=7.12 Hz, 2H), 3.69 (s, 1H), 2.75 (m, 2H), 2.64 (s, 3H), 2.49 (m, 2H), 2.28 (s, 3H), 1.51 ppm (t, J=7.12 Hz, 3H); ^{13}C NMR ($CDCl_3$, 100 MHz): δ=172.6, 163.0, 160.4, 140.7, 135.8, 133.3, 131.3, 130.5, 128.5, 127.9, 126.3, 123.9, 118.7, 118.3, 61.4, 51.8, 33.6, 19.4, 14.3, 13.5, 9.6 ppm; MALDI-TOF: m/z calcd for $C_{22}H_{23}BF_2N_2O_4$ [M^+] 428.224; found: 428.24.

Crystal data: Diffraction data were collected at low temperature on either a Nonius KappaCCD diffractometer equipped with $Mo_{K\alpha}$ radiation (λ=0.71073 Å) or a Bruker Kappa Apex-II diffractometer equipped with $Cu_{K\alpha}$ radiation (λ=1.54178 Å). Refinement was by full-matrix least squares using SHELXL, with hydrogen atoms in idealized positions, except for NH hydrogen atoms, which were located by difference maps and in most cases their positions refined. Disorder is present in several of the structures.

Crystal data for ***2a***: $C_{23}H_{30}N_2O_4$, monoclinic space group $P2_1/c$, a= 8.3020(6), b=18.1194(14), c=13.5258(10) Å, β=98.449(5)°, V= 2012.6(3) Å^3, T=90.0(5) K, Z=4, ρ_{calcd}=1.315 g cm^{-3}, $\mu(Cu_{K\alpha})$= 0.73 mm^{-1}. A total of 13,289 data was collected at to θ=69.0°. R=0.062 for 2895 data with $I>2\sigma(I)$ of 3597 unique data and 270 refined parameters.

Crystal data for ***2b*** *EtOAc solvate*: $C_{29}H_{34}N_2O_4{\cdot}1/2\,C_4H_8O_2$, triclinic space group $P\bar{1}$, a=8.698(3), b=14.961(5), c=21.472(9) Å, α=86.86(3), β= 88.15(2), γ=89.83(2)°, V=2788.5(18) Å^3, T=90.0(5) K, Z=4, ρ_{calcd}= 1.235 g cm^{-3}, $\mu(Cu_{K\alpha})$=0.67 mm^{-1}. 24,515 total data, θ_{max}=58.8°. R= 0.087 for 3895 data with $I>2\sigma(I)$ of 7545 unique data and 692 refined parameters.

Crystal data for ***2c*** *pentafluorobenzaldehyde co-crystal*: $C_{29}H_{29}F_5N_2O_4{\cdot}1/2\,C_7HF_5O$, tetragonal space group $I4_1/a$, a=24.931(2), c=40.838(4) Å, V=25,383(4) Å^3, T=90.0(5) K, Z=32, ρ_{calcd}=1.387 g cm^{-3}, $\mu(Cu_{K\alpha})$=

 © 2012 Wiley-VCH Verlag GmbH & Co. KGaA, Weinheim

1.06 mm^{-1}. 95523 total data, $\theta_{max}=68.9°$. $R=0.068$ for 8230 data with $I>2\sigma(I)$ of 11630 unique data and 838 refined parameters.

Crystal data for **2d**: $C_{30}H_{36}N_2O_5$, triclinic space group $P\bar{1}$, $a=10.7765(10)$, $b=11.1382(12)$, $c=14.2929(13)$ Å, $\alpha=100.304(5)$, $\beta=103.378(4)$, $\gamma=102.828(4)°$, $V=1578.7(3)$ Å^3, $T=90.0(5)$ K, $Z=2$, $\rho_{calcd}=1.189$ g cm^{-3}, $\mu(Cu_{K\alpha})=0.58$ mm^{-1}. 17121 total data, $\theta_{max}=68.4°$. $R=0.060$ for 4767 data with $I>2\sigma(I)$ of 5533 unique data and 354 refined parameters.

Crystal data for **3b**: $C_{29}H_{31}BF_2N_2O_4$, monoclinic space group $P2_1/c$, $a=11.3252(15)$, $b=24.088(5)$, $c=9.778(2)$ Å, $\beta=108.409(10)°$, $V=2530.9(8)$ Å^3, $T=150.0(5)$ K, $Z=4$, $\rho_{calcd}=1.366$ g cm^{-3}, $\mu(Mo_{K\alpha})=0.10$ mm^{-1}. 8398 total data, $\theta_{max}=27.9°$. $R=0.053$ for 3731 data with $I>2\sigma(I)$ of 6018 unique data and 392 refined parameters.

Crystal data for **3c**: $C_{29}H_{26}BF_7N_2O_4$, triclinic space group $P\bar{1}$, $a=8.0664(4)$, $b=14.5015(6)$, $c=23.4495(12)$ Å, $\alpha=92.042(4)$, $\beta=97.547(4)$, $\gamma=91.775(3)°$, $V=2715.8(2)$ Å^3, $T=90.0(5)$ K, $Z=4$, $\rho_{calcd}=1.493$ g cm^{-3}, $\mu(Cu_{K\alpha})=1.14$ mm^{-1}. 27216 total data, $\theta_{max}=60.3°$. $R=0.063$ for 4428 data with $I>2\sigma(I)$ of 8054 unique data and 780 refined parameters.

Crystal data for **3d**: $C_{30}H_{33}BF_2N_2O_5$, monoclinic space group $C2/c$, $a=25.927(2)$, $b=8.7936(10)$, $c=25.782(2)$ Å, $\beta=114.472(5)°$, $V=5350.0(8)$ Å^3, $T=90.0(5)$ K, $Z=8$, $\rho_{calcd}=1.367$ g cm^{-3}, $\mu(Cu_{K\alpha})=0.84$ mm^{-1}. 13921 total data, $\theta_{max}=68.3°$. $R=0.039$ for 4024 data with $I>2\sigma(I)$ of 4767 unique data and 364 refined parameters.

Crystal data for **3e**: $C_{31}H_{33}BF_2N_2O_6$, monoclinic space group $C2/c$, $a=41.881(3)$, $b=15.0780(15)$, $c=27.105(2)$ Å, $\beta=97.579(5)°$, $V=16{,}967(2)$ Å^3, $T=150.0(5)$ K, $Z=24$, $\rho_{calcd}=1.359$ g cm^{-3}, $\mu(Cu_{K\alpha})=0.85$ mm^{-1}. 64554 total data, $\theta_{max}=68.4°$. $R=0.043$ for 11391 data with $I>2\sigma(I)$ of 15206 unique data and 1150 refined parameters.

Crystal data for **4b**: $C_{29}H_{23}BF_2N_2O_4$, orthorhombic space group $Pbca$, $a=13.0867(9)$, $b=23.649(2)$, $c=15.7556(10)$ Å, $V=4876.2(6)$ Å^3, $T=100.0(5)$ K, $Z=8$, $\rho_{calcd}=1.396$ g cm^{-3}, $\mu(Cu_{K\alpha})=0.86$ mm^{-1}. 43,842 total data, $\theta_{max}=68.3°$. $R=0.036$ for 3670 data with $I>2\sigma(I)$ of 4434 unique data and 345 refined parameters.

Crystal data for **4d**: $C_{30}H_{25}BF_2N_2O_5$, orthorhombic space group $Pbca$, $a=16.208(3)$, $b=12.384(2)$, $c=24.802(4)$ Å, $V=4978.3(15)$ Å^3, $T=90.0(5)$ K, $Z=8$, $\rho_{calcd}=1.447$ g cm^{-3}, $\mu(Cu_{K\alpha})=0.90$ mm^{-1}. 30190 total data, $\theta_{max}=58.9°$. $R=0.063$ for 2995 data with $I>2\sigma(I)$ of 3557 unique data and 397 refined parameters.

Crystal data for **4e**: $C_{31}H_{25}BF_2N_2O_6$, orthorhombic space group $Pbca$, $a=15.792(2)$, $b=12.530(2)$, $c=26.067(4)$ Å, $V=5158.0(13)$ Å^3, $T=90.0(5)$ K, $Z=8$, $\rho_{calcd}=1.469$ g cm^{-3}, $\mu(Cu_{K\alpha})=0.93$ mm^{-1}. 34135 total data, $\theta_{max}=60.3°$. $R=0.078$ for 2405 data with $I>2\sigma(I)$ of 3788 unique data and 382 refined parameters.

Crystal data for **8**: $C_{22}H_{23}BF_2N_2O_4$, monoclinic space group $P2_1/n$, $a=11.4027(15)$, $b=7.3503(10)$, $c=24.381(3)$ Å, $\beta=102.545(6)°$, $V=1994.7(5)$ Å^3, $T=100.0(5)$ K, $Z=4$, $\rho_{calcd}=1.426$ g cm^{-3}, $\mu(Mo_{K\alpha})=0.11$ mm^{-1}. 22120 total data, $\theta_{max}=27.8°$. $R=0.039$ for 3415 data with $I>2\sigma(I)$ of 4679 unique data and 285 refined parameters.

Crystal data for **5b** *hexanes solvate*: $C_{29}H_{24}N_2O_4{\cdot}0.2\,C_6H_{14}$, monoclinic space group $C2/c$, $a=18.5304(12)$, $b=20.7226(14)$, $c=6.8836(4)$ Å, $\beta=108.738(4)°$, $V=2503.2(3)$ Å^3, $T=90.0(5)$ K, $Z=4$, $\rho_{calcd}=1.285$ g cm^{-3}, $\mu(Mo_{K\alpha})=0.09$ mm^{-1}. 10372 total data, $\theta_{max}=26.0°$. $R=0.047$ for 1634 data with $I>2\sigma(I)$ of 2478 unique data and 162 refined parameters.

Crystal data for **5b** *precursor*: $C_{29}H_{32}N_2O_4$, triclinic space group $P\bar{1}$, $a=8.5674(5)$, $b=11.1537(9)$, $c=13.4356(10)$ Å, $\alpha=69.244(5)$, $\beta=89.897(4)$, $\gamma=81.625(4)°$, $V=1186.03(15)$ Å^3, $T=90.0(5)$ K, $Z=2$, $\rho_{calcd}=1.323$ g cm^{-3}, $\mu(Cu_{K\alpha})=0.70$ mm^{-1}. 14723 total data, $\theta_{max}=69.3°$. $R=0.038$ for 3608 data with $I>2\sigma(I)$ of 4248 unique data and 349 refined parameters.

Crystal data for **5c**: $C_{29}H_{19}F_5N_2O_4$, monoclinic space group $P2_1/c$, $a=15.3125(15)$, $b=11.0509(10)$, $c=15.6714(15)$ Å, $\beta=115.117(5)°$, $V=2401.1(4)$ Å^3, $T=90.0(5)$ K, $Z=4$, $\rho_{calcd}=1.534$ g cm^{-3}, $\mu(Cu_{K\alpha})=1.11$ mm^{-1}. 17798 total data, $\theta_{max}=68.7°$. $R=0.034$ for 3953 data with $I>2\sigma(I)$ of 4323 unique data and 367 refined parameters.

Crystal data for **5c** *precursor*: $C_{29}H_{27}F_5N_2O_4$, monoclinic space group $P2_1/n$, $a=8.9739(5)$, $b=24.788(2)$, $c=11.3754(10)$ Å, $\beta=100.947(5)°$, $V=22484.4(3)$ Å^3, $T=90.0(5)$ K, $Z=4$, $\rho_{calcd}=1.504$ g cm^{-3}, $\mu(Cu_{K\alpha})=1.08$ mm^{-1}. 26194 total data, $\theta_{max}=68.6°$. $R=0.034$ for 3823 data with $I>2\sigma(I)$ of 4508 unique data and 367 refined parameters.

Crystal data for **5d**: $C_{30}H_{26}N_2O_5$, monoclinic space group $P2_1/n$, $a=9.456(2)$, $b=13.896(3)$, $c=18.304(4)$ Å, $\beta=93.890(15)°$, $V=93.890(15)$ Å^3, $T=90.0(5)$ K, $Z=4$, $\rho_{calcd}=1.369$ g cm^{-3}, $\mu(Mo_{K\alpha})=0.09$ mm^{-1}. 14344 total data, $\theta_{max}=26.0°$. $R=0.051$ for 3109 data with $I>2\sigma(I)$ of 4714 unique data and 339 refined parameters.

Crystal data for **5d** *precursor*: $C_{30}H_{34}N_2O_5$, orthorhombic space group $Pbca$, $a=21.665(2)$, $b=9.1272(10)$, $c=26.015(2)$ Å, $V=5144.2(8)$ Å^3, $T=90.0(5)$ K, $Z=8$, $\rho_{calcd}=1.298$ g cm^{-3}, $\mu(Cu_{K\alpha})=0.71$ mm^{-1}. 49,707 total data, $\theta_{max}=59.0°$. $R=0.034$ for 3043 data with $I>2\sigma(I)$ of 3696 unique data and 345 refined parameters.

CCDC-839637 (**2a**), CCDC-839638 (**2b**), CCDC-839639 (**2c**), CCDC-839640 (**2d**), CCDC-840083 (**3c**), CCDC-840084 (**3b**), CCDC-840085 (**3d**), CCDC-840086 (**3e**), CCDC-840120 (**4b**), CCDC-840121 (**4d**), CCDC-840122 (**4e**), CCDC-840123 (**8**), CCDC-840124 (**5b**), CCDC-840125 (**5b** precursor), CCDC-840126 (**5c**), CCDC-840127 (**5c** precursor), CCDC-840128 (**5d**), and CCDC-840129 (**5d** precursor) contain the supplementary crystallographic data for this paper. These data can be obtained free of charge from The Cambridge Crystallographic Data Centre via www.ccdc.cam.ac.uk/data_request/cif.

Computation modeling. The two reaction routes A and B were studied computationally in the framework of density functional theory.[35] The hybrid density functional B3LYP[36] was used at the 6–31G(d,p) level. The geometry of compounds **2b–e**, **2′b–e**, **3b–e**, **4b–e**, and **5b–e** were optimized and the relative energies were evaluated. Potential energy surface minima were confirmed with frequency calculations. The solvent effects were accounted for using the Polarizable Continuum Model (PCM).[37] The molecular electrostatic potentials at the atomic nuclei were calculated according to the literature.[38] All calculations were performed using Gaussian 09 program package.[39]

Steady-state absorption and fluorescence spectroscopy: The absorption measurements were carried out on a Varian Cary 50 UV/Vis spectrophotometer and the steady-state fluorescence spectroscopic studies in dichloromethane and methanol were performed on a PTI Quantum Master4/2006SE spectrofluorimeter, and in toluene on a Fluorolog®-3 Modular spectrofluorometer. For the fluorescence quantum yield measurements, dilute solutions with absorbance between 0.04–0.06 at the excitation wavelength were used. The fluorescence quantum yields of BODIPYs **7** and **3a–e** were obtained by comparing the area under the corrected emission spectrum of the test sample with that of rhodamine 6G (0.80 in methanol). For BODIPYs **4a–e** and **8**, methylene blue (0.03 in methanol) and cresyl violet perchlorate (0.54 in ethanol) were used as external standards, respectively.[29] All spectra were recorded at room temperature using non-degassed samples, spectroscopic grade solvents and a 10 mm quartz cuvette. In all cases, correction for the refractive index was applied.

Cell culture. All tissue culture media and reagents were obtained from Invitrogen. Human carcinoma HEp2 cells were obtained from ATCC and maintained in a 50:50 mixture of DMEM:Advanced MEM containing 5% FBS. The HEp2 cells were sub-cultured biweekly to maintain sub-confluent stocks. the 4th to 15th passage cells were used for all the experiments.

Time-dependent cellular uptake: The HEp2 cells were plated at 7500 per well in a Costar 96 well plate and allowed to grow for 36 h. BODIPY stocks were prepared in DMSO containing 1% Cremophor EL, at a concentration of 32 mM and then diluted into medium to final working concentrations. The cells were exposed to 10 μM of each BODIPY for 0, 1, 2, 4, 8, and 24 h. At the end of the incubation time period the loading medium was removed and the cells were washed with 200 μL of PBS. The cells were solubilized upon addition of 100 μL of 0.25% Triton X-100 (Calbiochem) in PBS. To determine the BODIPY concentration, fluorescence emission was read at 570/670 nm (excitation/emission) using a BMG FLUOstar plate reader. The cell numbers were quantified by the CyQuant cell proliferation assay (Invitrogen) as per the manufacturer's instructions, and the uptake was expressed in terms of nM compound per cell.

 © 2012 Wiley-VCH Verlag GmbH & Co. KGaA, Weinheim

Cytotoxicity: For the dark toxicity, the HEp2 cells were plated as described above and allowed 36–48 h to attach. The cells were exposed to increasing concentrations of BODIPY up to 400 μM and incubated overnight. The loading medium was then removed and medium containing Cell Titer Blue (Promega) as per the manufacturer's instructions was added to the cells. Cell viability was then measured by reading the fluorescence at 570/615 nm using a BMG FLUOstar plate reader. The signal was normalized to 100% viable (untreated) cells and 0% viable (treated with 0.2% saponin) cells. For the phototoxicity, the HEp2 cells were prepared as described above for the dark cytotoxicity assay and treated with BODIPY concentrations of 0, 6.25, 12.5, 25, 50 and 100 μM. After compound loading overnight, the medium was removed and replaced with medium containing 50 mM HEPES pH 7.4. The cells were exposed to a NewPort light system with 175 W halogen lamp for 20 min, filtered through a water filter to provide approximated 1.5 $J\,cm^{-2}$ light dose. The cells were kept cool by placing the culture on a 5°C Echotherm chilling/heating plate (Torrey Pines Scientific, Inc.). The cells were returned to the incubator overnight and assayed for viability as described above for the dark cytotoxicity experiment.

Microscopy: The cells were incubated in a glass bottom 6-well plate (MatTek) and allowed to grow for 48 h. The cells were then exposed to 10 μM of each BODIPY for 6 h. Organelle tracers were obtained from Invitrogen and used at the following concentrations: LysoSensor Green 50 nM, MitoTracker Green 250 nM, ER Tracker Blue/white 100 nM, and BODIPY FL C5 Ceramide 1 μM. The organelle tracers were diluted in medium and the cells were incubated concurrently with BODIPY and tracers for 30 min before washing 3 times with PBS and microscopy. Images were acquired using a Leica DMRXA microscope with 40× NA 0.8dip objective lens and DAPI, GFP and Texas Red filter cubes (Chroma Technologies).

Acknowledgements

This work was supported by the National Science Foundation (Grant CHE-0611629). We are thankful to Dr. Azeem Hassam for assistance with mass spectrometry analysis. The authors thank the Louisiana Optical Network Initiative for the use of their computer facilities and the Clare Boothe Luce Foundation for providing a scholarship for SM.

[1] a) G. Ulrich, R. Ziessel, A. Harriman, *Angew. Chem.* **2008**, *120*, 1202–1219; *Angew. Chem. Int. Ed.* **2008**, *47*, 1184–1201; b) R. Ziessel, G. Ulrich, A. Harriman, *New J. Chem.* **2007**, *31*, 496–501; c) M. Benstead, G. H. Mehl, R. W. Boyle, *Tetrahedron* **2011**, *67*, 3573–3601.

[2] Z. Shen, H. Rohr, K. Rurack, H. Uno, M. Spieles, B. Schulz, G. Reck, N. Ono, *Chem. Eur. J.* **2004**, *10*, 4853–4871.

[3] a) A. Loudet, K. Burgess, *Chem. Rev.* **2007**, *107*, 4891–4932; b) http://probes.invitrogen.com, Molecular Probes, Invitrogen Corporation, **2006**.

[4] a) K. Krumova, P. Oleynik, P. Karam, G. Cosa, *J. Org. Chem.* **2009**, *74*, 3641–3651; b) T. W. Hudnall, F. P. Gabbai, *Chem. Commun.* **2008**, 4596–4597; c) X. Peng, J. Du, J. Fan, J. Wang, Y. Wu, J. Zhao, S. Sun, T. Xu, *J. Am. Chem. Soc.* **2007**, *129*, 1500–1501; d) A. Coskun, E. U. Akkaya, *J. Am. Chem. Soc.* **2006**, *128*, 14474–14475.

[5] a) H. Kobayashi, M. Ogawa, R. Alford, P. L. Choyle, Y. Urano, *Chem. Rev.* **2010**, *110*, 2620–2640; b) C. Peters, A. Billich, M. Ghobrial, K. Hoegenauer, T. Ullrich, P. Nussbaumber, *J. Org. Chem.* **2007**, *72*, 1842–1845; c) Z. Li, E. Mintzer, R. Bittman, *J. Org. Chem.* **2006**, *71*, 1718–1721.

[6] a) S. Mula, A. K. Ray, M. Banerjee, T. Chaudhuri, K. Dasgupta, S. Chattopadhyay, *J. Org. Chem.* **2008**, *73*, 2146–2154; b) T. Rousseau, A. Cravino, T. Bura, G. Ulrich, R. Ziessel, J. Roncali, *Chem. Commun.* **2009**, 1673–1675; c) A. Harriman, R. Ziessel, *Chem. Eur. J.* **2008**, *14*, 11461–11473.

[7] a) Y.-W. Wang, A. B. Descalzo, Z. Shen, X.-Z. You, K. Rurack, *Chem. Eur. J.* **2010**, *16*, 2887–2903; b) R. Ziessel, L. Bonardi, G. Ulrich, *Dalton Trans.* **2006**, 2913–2918; c) Y. Yamada, Y. Tomiyama, A. Morita, M. Ikekita, S. Aoki, *ChemBioChem* **2008**, *9*, 853–856; d) L. Jiao, J. Li, S. Zhang, C. Wei, E. Hao, M. G. H. Vicente, *New J. Chem.* **2009**, *33*, 1888–1893.

[8] J. A. Jacobsen, J. R. Stork, D. Magde, S. M. Cohen, *Dalton Trans.* **2010**, *39*, 957–968.

[9] a) M. Tasior, J. Murtagh, D. O. Frimannsson, S. O. McDonnell, D. F. O'Shea, *Org. Biomol. Chem.* **2010**, *8*, 522–525; b) Y. Li, D. Dolphin, B. O. Patrick, *Tetrahedron Lett.* **2010**, *51*, 811–814; c) W. Zhao, E. M. Carriera, *Chem. Eur. J.* **2006**, *12*, 7254–7263; d) W. Zhao, E. M. Carriera, *Angew. Chem.* **2005**, *117*, 1705–1707; *Angew. Chem. Int. Ed.* **2005**, *44*, 1677–1679; e) J. Killoran, L. Allen, J. F. Gallagher, W. M. Gallagher, D. F. O'Shea, *Chem. Commun.* **2002**, 1862–1863.

[10] a) T. Rohand, M. Baruah, W. Qin, N. Boens, W. Dehaen, *Chem. Commun.* **2006**, 266–268; b) T. Rohand, W. Qin, N. Boens, W. Dehaen, *Eur. J. Org. Chem.* **2006**, 4658–4663; c) J. Han, O. Gonzalez, A. Aquilar-Aquilsr, E. Pena-Carera, K. Burgess, *Org. Biomol. Chem.* **2009**, *7*, 34–36; d) L. Li, B. Nguyen, K. Burgess, *Bioorg. Med. Chem. Lett.* **2008**, *18*, 3112–3116; e) K. Rurack, M. Kollmannsberger, J. Daub, *New J. Chem.* **2001**, *25*, 289–292.

[11] a) T. Okujima, Y. Tomimori, J. Nakamura, H. Yamada, H. Uno, N. Ono, *Tetrahedron* **2010**, *66*, 6895–6900; b) Y. Kubo, Y. Minowa, T. Shoda, K. Takeshita, *Tetrahedron Lett.* **2010**, *51*, 1600–1602; c) M. Bröring, R. Kruger, S. Link, C. Kleeber, S. Kohler, X. Xie, B. Ventura, L. Flamigni, *Chem. Eur. J.* **2008**, *14*, 2976–2983.

[12] a) L. Jiao, C. Yu, M. Liu, Y. Wu, K. Cong, T. Meng, Y. Wang, E. Hao, *J. Org. Chem.* **2010**, *75*, 6035–6038; b) A. B. Descalzo, H.-J. Xu, Z.-L. Xue, K. Hoffmann, Z. Shen, M. G. Weller, X.-Z. You, K. Rurack, *Org. Lett.* **2008**, *10*, 1581–1584.

[13] L. Zeng, E. W. Miller, A. Pralle, E. Y. Isacoff, C. J. L. Chang, *J. Am. Chem. Soc.* **2006**, *128*, 10–11.

[14] M. A. Filatov, A. V. Cheprakov, I. P. Beletskaya, *Eur. J. Org. Chem.* **2007**, 3468–3475.

[15] M. A. Filatov, A. Y. Lebedev, S. N. Mukhin, S. A. Vinogradov, A. V. Cheprakov, *J. Am. Chem. Soc.* **2010**, *132*, 9552–9554.

[16] G. Ulrich, S. Goeb, A. De Nicola, P. Retailleau, R. Ziessel, *J. Org. Chem.* **2011**, *76*, 4489–4505.

[17] a) S. I. Zav'yalov, T. I. Skoblik, *Bull. Acad. Sci. USSR Div. Chem. Sci. (Engl. Transl.)* **1977**, *26*, 2559–2562; b) C. J. Medforth, M. D. Berber, K. M. Smith, J. Shelnutt, *Tetrahedron Lett.* **1990**, *31*, 3719–3722; c) D. A. May, *J. Org. Chem.* **1992**, *57*, 4820–4828; d) M. A. Filatov, A. Y. Lebedev, S. A. Vinogradov, A. V. Cheprakov, *J. Org. Chem.* **2008**, *73*, 4175–4185.

[18] D. A. Lee, K. M. Smith, *J. Chem. Soc. Perkin Trans. 1* **1997**, 1215–1227.

[19] J. H. P. Utley, G. G. Rozenberg, *Tetrahedron* **2002**, *58*, 5251–5265.

[20] O. S. Finikova, A. V. Cheprakov, I. P. Beletskaya, P. J. Carroll, S. A. Vinogradov, *J. Org. Chem.* **2004**, *69*, 522–535.

[21] a) A. Burghart, H. Kim, M. B. Welch, L. H. Thoresen, J. Reibenspies, K. Burgess, *J. Org. Chem.* **1999**, *64*, 7813–7819; b) L. Wu, K. Burgess, *Chem. Commun.* **2008**, 4933–4935.

[22] a) J. A. P. Baptista de Almeida, G. W. Kenner, J. Rimmer, K. M. Smith, *Tetrahedron* **1976**, *32*, 1793–1799; b) K. M. Smith, G. W. Craig, *J. Org. Chem.* **1983**, *48*, 4302–4306.

[23] a) F. López Arbeloa, J. Bañuelos Prieto, V. Martínez Martínez, T. Arbeloa López, I. López Arbeloa, *ChemPhysChem* **2004**, *5*, 1762–1771; b) T. López Arbeloa, F. López Arbeloa, I. López Arbeloa, I. Garcia-Moreno, A. Costela, R. Sastre, F. Amat-Guerri, *Chem. Phys. Lett.* **1999**, *299*, 315–321; c) M. Kollmannsberger, K. Rurack, U. Resch-Genger, J. Daub, *J. Phys. Chem. A* **1998**, *102*, 10211–10220.

[24] O. Galangau, C. Dumas-Verdes, R. Meallet-Renault, G. Clavier, *Org. Biomol. Chem.* **2010**, *8*, 4546–4553.

[25] a) W. Qin, M. Baruah, M. V. Auweraer, F. C. De Schryver, N. Boens, *J. Phys. Chem. A* **2005**, *109*, 7371–7384; b) G. Meng, S. Velayudham, A. Smith, R. Luck, H. Liu, *Macromolecules* **2009**, *42*, 1995–2001.

[26] I. J. Arroyo, R. Hu, G. Merino, B. Z. Tang, E. P. Cabera, *J. Org. Chem.* **2009**, *74*, 5719–5722.

[27] a) H. L. Kee, C. Kirmaier, L. Yu, P. Thamyongkit, W. J. Youngblood, M. E. Calder, L. Ramos, B. C. Noll, D. F. Bocian, W. R. Scheidt,

 © 2012 Wiley-VCH Verlag GmbH & Co. KGaA, Weinheim

R. R. Birge, J. S. Lindsey, D. Holten, *J. Phys. Chem. B* **2005**, *109*, 20433–20443; b) R. Hu, E. Lager, A. Aguilar-Aguilar, J. Liu, J. W. Y. Lam, H. H. Y. Sung, I. D. Williams, Y. Zhong, K. S. Wong, E. Peña-Cabrera, B. Z. Tang, *J. Phys. Chem. C* **2009**, *113*, 15845–15853.

[28] G. Vives, C. Giansante, R. Bofinger, G. Raffy, A. D. Guerzo, B. Kauffmann, P. Batat, G. Jonusauskasc, N. D. McClenaghan, *Chem. Commun.* **2011**, *47*, 10425–10427.

[29] J. Olmsted, *J Phys. Chem.* **1979**, *83*, 2581–2584.

[30] a) E. Hao, T. J. Jensen, B. H. Courtney, M. G. H. Vicente, *Bioconjugate Chem.* **2005**, *16*, 1495–1502; b) W. Liu, T. J. Jensen, F. R. Fronczek, R. P. Hammer, K. M. Smith, M. G. H. Vicente, *J. Med. Chem.* **2005**, *48*, 1033–1041.

[31] S. H. Lim, C. Thivierge, P. Nowak-Sliwinska, J. Han, H. van den Bergh, G. Wagnieres, K. Burgess, H. B. Lee, *J. Med. Chem.* **2010**, *53*, 2865–2874.

[32] a) H.-J. Böhm, D. Banner, S. Bendels, M. Kansy, B. Kuhn, K. Müller, U. Obst-Sander, M. Stahl, *ChemBioChem* **2004**, *5*, 637–643; b) J. C. Biffinger, H. W. Kim, S. G. DiMagno, *ChemBioChem* **2004**, *5*, 622–627.

[33] L. Jiao, C. Yu, T. Uppal, M. Liu, Y. Li, Y. Zhou, E. Hao, X. Hu, M. G. H. Vicente, *Org. Biomol. Chem.* **2010**, *8*, 2517–2519.

[34] Q. Zheng, G. Xu, P. N. Prasad, *Chem. Eur. J.* **2008**, *14*, 5812–5819.

[35] P. Hohenberg, W. Kohn, *Phys. Rev.* **1964**, *136*, B864-B871.

[36] a) A. D. Becke, *J. Chem. Phys.* **1993**, *98*, 5648–5652; b) C. Lee, W. Yang, R. G. Parr, *Phys. Rev. B* **1988**, *37*, 785–789.

[37] a) S. Miertuš, E. Scrocco, J. Tomasi, *Chem. Phys.* **1981**, *55*, 117–129; b) J. Tomasi, B. Mennucci, R. Cammi, *Chem. Rev.* **2005**, *105*, 2999–3093.

[38] a) P. Politzer, In *Chemical Applications of Atomic and Molecular Electrostatic Potentials* (Eds.: P. Politzer, D. G. Truhlar), Plenum, New York, **1981**, p. 7; b) B. Galabov, P. Bobadova-Parvanova, *J. Phys. Chem. A* **1999**, *103*, 6793–6799.

[39] Gaussian 2009, M. J. Frisch, G. W. Trucks, H. B. Schlegel, M. A. Robb, J. R. Cheeseman, G. Scalmani, V. Barone, B. Mennucci, G. A. Petersson, H. Nakatsuji, M. Caricato, X. Li, H. P. Hratchian, A. F. Izmaylov, J. Bloino, G. Zheng, J. L. Sonnenberg, M. Hada, M. Ehara, K. Toyota, R. Fukuda, J. Hasegawa, M. Ishida, T. Nakajima, Y. Honda, O. Kitao, H. Nakai, T. Vreven, J. A. Montgomery, J. E. Peralta, F. Ogliaro, M. Bearpark, J. J. Heyd, E. Brothers, K. N. Kudin, V. N. Staroverov, R. Kobayashi, J. Normand, K. Raghavachari, N. Rendell, J. C. Burant, S. S. Iyengar, J. Tomasi, M. Cossi, N. Rega, J. M. Millam, N. Klene, J. E. Knox, J. B. Cross, V. Bakken, C. Adamo, J. Jaramillo, R. Gomperts, R. E. Stratmann, O. Yazyev, A. J. Austin, R. Cammi, C. Pomelli, J. W. Ochterski, R. L. Martin, K. Morokuma, V. G. Zakrzewski, G. A. Voth, P. Salvador, J. J. Dannenberg, S. Dapprich, A. D. Daniels, O. Farkas, J. B. Foresman, J. B. Ortiz, J. Cioslowski, D. J. Fox, Gaussian, Inc., Wallingford CT, **2009**.

Received: September 23, 2011
Published online: February 24, 2012

 © 2012 Wiley-VCH Verlag GmbH & Co. KGaA, Weinheim